


Nanoparticle-assisted, image-guided laser interstitial thermal therapy for cancer treatment

Sumiao Pang¹ | Anshika Kapur² | Keri Zhou¹ | Pavlos Anastasiadis^{2,3} |
Nicholas Ballirano¹ | Anthony J. Kim^{2,3} | Jeffrey A. Winkles^{2,3} |
Graeme F. Woodworth^{2,3} | Huang-Chiao Huang^{1,3} 

¹Fischell Department of Bioengineering, University of Maryland at College Park, College Park, Maryland, USA

²Department of Neurosurgery, University of Maryland School of Medicine, Baltimore, Maryland, USA

³University of Maryland Marlene and Stewart Greenebaum Cancer Center, Baltimore, Maryland, USA

Correspondence

Huang-Chiao Huang, Fischell Department of Bioengineering, University of Maryland at College Park, College Park, MD, USA.

Email: hchuang@umd.edu

Funding information

A. James Clark School of Engineering; University of Maryland Neuro-Link Grant; National Institutes of Health, Grant/Award Numbers: R01NS107813, R21EB028508

Edited by: Silvia Muro, Associate Editor and Gregory Lanza, Co-Editor-in-Chief

Abstract

Laser interstitial thermal therapy (LITT) guided by magnetic resonance imaging (MRI) is a new treatment option for patients with brain and non-central nervous system (non-CNS) tumors. MRI guidance allows for precise placement of optical fiber in the tumor, while MR thermometry provides real-time monitoring and assessment of thermal doses during the procedure. Despite promising clinical results, LITT complications relating to brain tumor procedures, such as hemorrhage, edema, seizures, and thermal injury to nearby healthy tissues, remain a significant concern. To address these complications, nanoparticles offer unique prospects for precise interstitial hyperthermia applications that increase heat transport within the tumor while reducing thermal impacts on neighboring healthy tissues. Furthermore, nanoparticles permit the co-delivery of therapeutic compounds that not only synergize with LITT, but can also improve overall effectiveness and safety. In addition, efficient heat-generating nanoparticles with unique optical properties can enhance LITT treatments through improved real-time imaging and thermal sensing. This review will focus on (1) types of inorganic and organic nanoparticles for LITT; (2) in vitro, in silico, and ex vivo studies that investigate nanoparticles' effect on light-tissue interactions; and (3) the role of nanoparticle formulations in advancing clinically relevant image-guided technologies for LITT.

This article is categorized under:

Therapeutic Approaches and Drug Discovery > Nanomedicine for Neurological Disease

Implantable Materials and Surgical Technologies > Nanoscale Tools and Techniques in Surgery

This is an open access article under the terms of the [Creative Commons Attribution-NonCommercial-NoDerivs](https://creativecommons.org/licenses/by-nc-nd/4.0/) License, which permits use and distribution in any medium, provided the original work is properly cited, the use is non-commercial and no modifications or adaptations are made.

© 2022 The Authors. *WIREs Nanomedicine and Nanobiotechnology* published by Wiley Periodicals LLC.

KEYWORDS

cancer, image guided, interstitial hyperthermia, laser interstitial thermal therapy, nanoparticles, optical fiber, tumor

1 | INTRODUCTION

Magnetic resonance imaging (MRI)-guided laser interstitial thermal therapy (LITT) is an emerging technology for treating brain and non-central nervous system (non-CNS) tumors. For brain tumors, LITT is performed by stereotactically inserting an optical fiber through a small burr hole (<5 mm) into the tumor and laser heating tissues to induce local hyperthermia and antitumor effects (T. R. Patel & Chiang, 2014). MRI guidance ensures accurate laser fiber positioning in the tumor, and MR thermometry allows real-time monitoring and assessment of thermal doses during the procedure. Currently, there are two FDA-approved LITT systems: the Visualase™ system uses a 15 W, 980 nm diode laser (P. Patel et al., 2016), and the Neuroblate™ system uses a 12 W, 1064 nm Nd:YAG laser (Kamath et al., 2017). These lasers have a tissue penetration depth of approximately 0.2–1 cm and can provide an effective treatment radius (also known as the central zone) of around 2–3 cm from the tip of the probe (Salem et al., 2019). Depending on the tumor's shape, geometry, and size, the tip can be moved along the implanted trajectory, or multiple trajectories may be used for larger tumors. Upon laser activation, photons are absorbed by tumor tissues and converted into thermal energy. When the temperature at the central zone reaches 50–80°C, protein denaturation and coagulative necrosis occur in a short amount of time (<10 min) (Salem et al., 2019). The peripheral zone surrounds the central zone, where prolonged heating (>10 min) at 43–45°C can lead to cytotoxic edema with irreversible cell damage. Such hyperthermic temperatures could also sensitize cancer cells to radiation and chemotherapy (Grauer et al., 2019; Man et al., 2015; Schneider et al., 2020). Beyond the peripheral zone lies viable cells, disrupted blood–brain barrier, and vasogenic edema that may take up to over a month to regress. In the clinic, LITT has been shown to improve the median overall survival time up to 20.9 months for patients with recurrent glioblastoma, compared to surgery and chemotherapy (11.1–16 months). However, complications of LITT, including hemorrhage, edema, seizures, and thermal injury to nearby tissues, remain a central challenge (Kim et al., 2020; Sharma et al., 2016; Sloan et al., 2013). Nanotechnology provides exceptional opportunities for applications of interstitial hyperthermia where heat transfer within the tumor can be improved and thermal effects on the surrounding cerebral tissues can be reduced. In addition to enhancing the effectiveness and safety of LITT, nanotechnology allows the co-delivery of therapeutic agents that can synergize with LITT. A proposed workflow for implementation of nanoparticles for brain tumor interstitial hyperthermia is shown in Figure 1. Ideally, if patients are qualified for this combination therapy, nanoparticles can be delivered intratumorally during a biopsy or right before LITT procedures. Alternatively, if patients have undergone a biopsy, the tissue samples can be used for screening of certain markers that could be advantageous for surface modified nanoparticle targeted approaches.

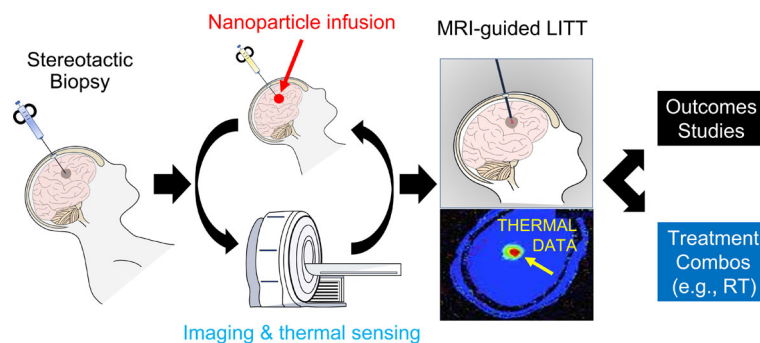


FIGURE 1 Envisioned clinical treatment paradigm. The envisioned clinical treatment paradigm builds from new and established neurosurgical workflows that enable streamlined nanoparticle infusion via intratumoral delivery during biopsy, postbiopsy, or right before laser interstitial thermal therapy (LITT) procedures. Post=nanoparticle infusion, intraoperative imaging-based feedback and intra-LITT magnetic resonance imaging (MRI)-based feedback can be leveraged for improved imaging, thermal sensing, and enhanced treatment. Thermal data image from Medvid et al. (2015).

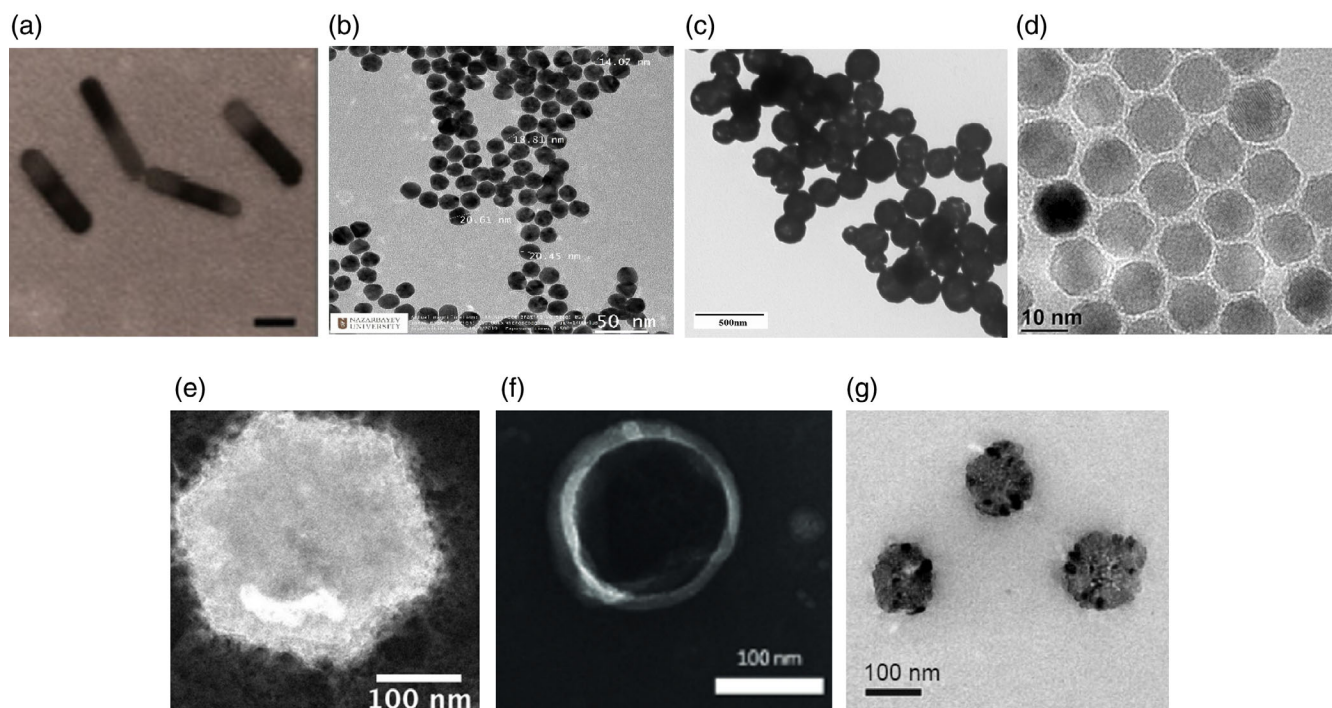


FIGURE 2 Transmission electron microscopy (TEM) images of inorganic and organic nanoparticles. A panel of TEM images showing the various nanoparticles that have been combined with interstitial light delivery. Inorganic nanoparticles: (a) gold nanorods (Bagley et al., 2013), (b) gold nanospheres (Ashikbayeva et al., 2020), (c) gold nanoshells (Leung et al., 2013), (d) magnetic iron oxide (Wierzbinski et al., 2018), (e) magnesium nanoparticles (Biggins et al., 2018). Organic nanoparticles: (f) porphyrins (MacDonald et al., 2014) and (g) liposome-gold nanoparticles (H. L. Huang et al., 2015). Scale for each image: 20, 50, 500, 10, 100, 100, and 100 nm, respectively.

A wide variety of organic and inorganic nanoparticles have been developed, and many of them can be used to improve the safety and efficacy of LITT. Figure 2 showcases representative transmission electron microscopy images for the types of nanoparticles that will be discussed in this review (Ashikbayeva et al., 2020; Bagley et al., 2013; Biggins et al., 2018; H. L. Huang et al., 2015; Leung et al., 2013; MacDonald et al., 2014; Wierzbinski et al., 2018). The most prominent inorganic nanoparticles are gold nanoparticles, formulated in different sizes and shapes (e.g., rods, shells, spheres, stars, and cages). Gold nanoparticles are generally easy to synthesize, biocompatible, and their unique surface plasmon resonance property allows efficient conversion of laser energy into heat (X. Huang et al., 2007; Stabile et al., 2020). Organic nanoparticles that are ideal for enhancing LITT include porphyrins, magnesium nanoparticles, and temperature sensitive liposomes loaded with gold nanoparticles (Ashikbayeva et al., 2020; H. L. Huang et al., 2015; Muhanna et al., 2015). The majority of nanoparticle formulations discussed in this review for assisting LITT are delivered intravenously; however, intratumoral delivery of these nanoparticles could be another route for possible enhanced LITT outcomes. The presence of nanoparticles may also allow for improved scattering effects by randomizing the reflection light paths, thereby further improving heat distribution profiles in tissues. This review also discusses several *in silico*, *in vitro*, and *ex vivo* studies that have investigated the impact of nanoparticles on light-tissue interaction. Besides their unique photophysical properties, nanoparticles can also be surface modified with other drugs and/or imaging agents for enhanced selectivity, effectiveness, and monitoring (imaging) of LITT *in vivo* (Knights et al., 2020; Ren et al., 2017).

2 | IORGANIC AND ORGANIC NANOPARTICLES STUDIED FOR LITT

2.1 | Inorganic nanoparticles

Gold nanoparticle-enhanced photothermal treatments can increase thermal conductance and capacitance within the tumor and reduce heat transfer to surrounding normal tissues (Dickerson et al., 2008; H. C. Huang et al., 2009, 2010;

Z. Qin & Bischof, 2012). Thus, gold nanoparticles are attractive nanoparticle agents for LITT; offering the opportunity to improve the efficacy and safety of LITT. As mentioned earlier, the morphology and size of gold nanoparticles can vary rendering them highly tunable for photothermal therapy (Y. Liu et al., 2015; Wu et al., 2010) but gold nanoshells, nanorods, and spheres have been studied mostly in combination with interstitial laser light delivery.

Gold nanoshells and gold nanorods can absorb light in the near-infrared (NIR) region (650–900 nm) and convert light into heat energy for localized cell destruction, mainly by apoptosis and/or necrosis (Bagley et al., 2013; Z. Qin & Bischof, 2012). For example, the intense absorption cross-sections (C_{abs}) of gold nanoshells (150 nm size) or gold nanorods (49 nm \times 13 nm size) excited at \sim 800 nm wavelength has C_{abs} of 4.57×10^5 and 5.67×10^3 nm², respectively. This is \sim 5 to 7 orders of magnitude *higher* than most organic molecular dyes (e.g., indocyanine green, $C_{\text{abs}} = 1.6 \times 10^{-2}$ nm² at \sim 800 nm), thus making them excellent candidates as heat generators for thermal therapy (Panchapakesan et al., 2011; Z. Qin & Bischof, 2012). NIR light penetrates human tissue from half a millimeter up to a few centimeters due to minimal absorption by water and blood in this region of the wavelength spectrum (Weissleder, 2001). When NIR light activates gold nanoparticles, the photons excite electrons within the gold nanoparticles to the higher electronic levels. These hot electrons relax energy by collision with the gold nanocrystal lattice, resulting in heating of the lattice phonons (e.g., electron–phonon interaction). The lattice phonon cools by dissipating its heat to surrounding tissues by phonon–phonon relaxation (Z. Qin & Bischof, 2012).

Gold nanoparticles can be easily synthesized and scaled up using the surfactant-assisted seed growth method, the most commonly used method for synthesizing gold nanorods and gold nanoshells. During the synthesis procedure, gold nanoshells' and gold nanorods' aspect ratios can be altered via core : shell (C:S) ratio and length: diameter (L:D) ratio, respectively (Loo et al., 2004; Nikoobakht & El-Sayed, 2003). This allows for the surface plasmon resonance wavelengths of these particles to be tunable in the NIR region. In addition to its easily tunable optical properties, gold nanoparticles' surface properties can be easily modified after synthesis to achieve unique targeting properties. Indeed, it is highly beneficial to specifically target nanoparticles to cancer cells to achieve safe and selective thermal treatments of tumors and minimize normal tissue damage. This can be accomplished via biofunctionalization by adding tumor receptor-specific antibodies that can increase nanoparticle binding to tumor cells that overexpress an antigen (Perez et al., 2016; Wadajkar et al., 2017).

Gold nanoparticles have also been conjugated with several different tumor receptor-specific antibodies and tested in cell culture studies, including anti-epidermal growth factor receptor (anti-EGFR) antibodies to target overexpressed EGFR in oral cancer cells, lung cancer, and cervical cancer cells (El-Sayed et al., 2006; X. Huang, El-Sayed, et al., 2006; X. Huang, Jain, et al., 2006; Knights et al., 2020), anti-human epidermal growth factor receptor-2 (Her2) antibodies to target overexpressed Her2 in breast cancer cells (Loo et al., 2005), and F19 antibodies to target overexpressed seprase antigen (human fibroblast activation protein α) in breast cancer cells (Zharov et al., 2005). Early studies reported by El-Sayed's group demonstrated that anti-EGFR-conjugated gold nanoparticles (\sim 40 nm in diameter) showed increased selectivity toward human oral squamous cell carcinoma (HSC 3 and HOC 313 cell lines) and not the noncancerous human keratinocytes (HaCaT cell line) in vitro. Selective binding with the anti-EGFR-conjugated gold nanoparticles requires only 150 and 200 mW laser power with a 1 mm diameter laser focal spot to achieve cell death. In comparison, the noncancerous cells require more than twice the laser power (450 mW), with all groups reaching temperatures over 70°C (X. Huang, Jain, et al., 2006).

In a 2005 study, Zharov and colleagues developed a novel approach of enhancing selective nanophotothermolysis via laser activation by using *gold nanoparticle clustering* methods (Zharov et al., 2005). Two clustering strategies were demonstrated, and the first one consisted of priming human breast adenocarcinoma cells (MDA-MB-231 cell line) in vitro with F19 monoclonal antibodies that selectively attached to the overexpressed seprase antigen and then incubating with 40-nm gold nanoparticles conjugated with goat anti-mouse immunoglobulin antibodies that selectively targeted the primary antibodies. The second clustering strategy used silver enhancement in nontoxic doses to promote clustering on the surface membrane. The laser treatment experiments used a Nd:YAG laser in Q-switched mode that delivered 532 or 805 nm wavelengths with a 12-ns pulse width and a continuous wave laser that delivered 514 and 805 nm wavelengths at 1 and 3 W with a 2-min exposure time for both (Zharov et al., 2005). The antibody-conjugated gold nanoparticles selectively targeted and accumulated onto cancer cell surfaces, thus forming large clusters averaging between 100 and 200 nm. The larger-sized gold nanoclusters resulted in a red-shift absorption peak and resulted in enhanced laser-induced cancer cell killing of resulting in less than 0.5% viable cells compared to nonclustering gold nanoparticles with more than 40% viable cells left after three laser pulses were applied at 532 nm (0.5 J cm^{-2}) for both (Zharov et al., 2005). In addition, optimal cell death was achieved when gold nanoclusters were inside the membrane via endocytic uptake. In a more recent study, Knights et al. used bright and dark field imaging to show that gold

nanorods ($L:D = 148:40$ nm) functionalized with mouse monoclonal anti-EGFR antibodies displayed cellular selectivity across all experimental groups using the lung cancer cell line (A549) in vitro (Figure 3a) at 4- and 24-h postincubation and postwash, compared to control gold nanorods that were not functionalized with the anti-EGFR antibodies (Figure 3b) (Knights et al., 2020). Washing each well postincubation was a critical step in this experimental setup due to the need to minimize the number of gold nanorods that remained unbound to the cell surface receptors so that only surface bound nanoparticles could be imaged. Furthermore, to quantify the impact of the imaged cellular selectivity, the study utilized two types of lasers with 854 nm wavelength that included a (i) pulse laser set to 10 Hz with a pulse duration of 7-ns, spot size of 9 mm and an average power of 160 mW, and (ii) continuous wave diode laser operating with a spot size of 9 mm and an average power of 950 mW. A standard MTT (3-[4,5-dimethylthiazol-2-yl]-2,5 diphenyl tetrazolium bromide) colorimetric assay was used to measure cell viability postlaser irradiation. Results showed that a 4-h incubation time was not adequate enough to achieve photothermal cancer cell death with both targeted and untargeted gold nanorods. However, the 24-h incubation time resulted in a much higher uptake of targeted gold nanorods achieving tumor cell death of 93% and 46% with the pulse and continuous wave laser, respectively. Both studies demonstrate the potential application of pulse wave lasers in combination with targeted gold nanoparticles and gold nanorods as an alternative laser ablation strategy for reducing undesired damage to surrounding tissues compared to continuous wave lasers that typically generates bulk heating effects. In addition, future work involving in vivo studies

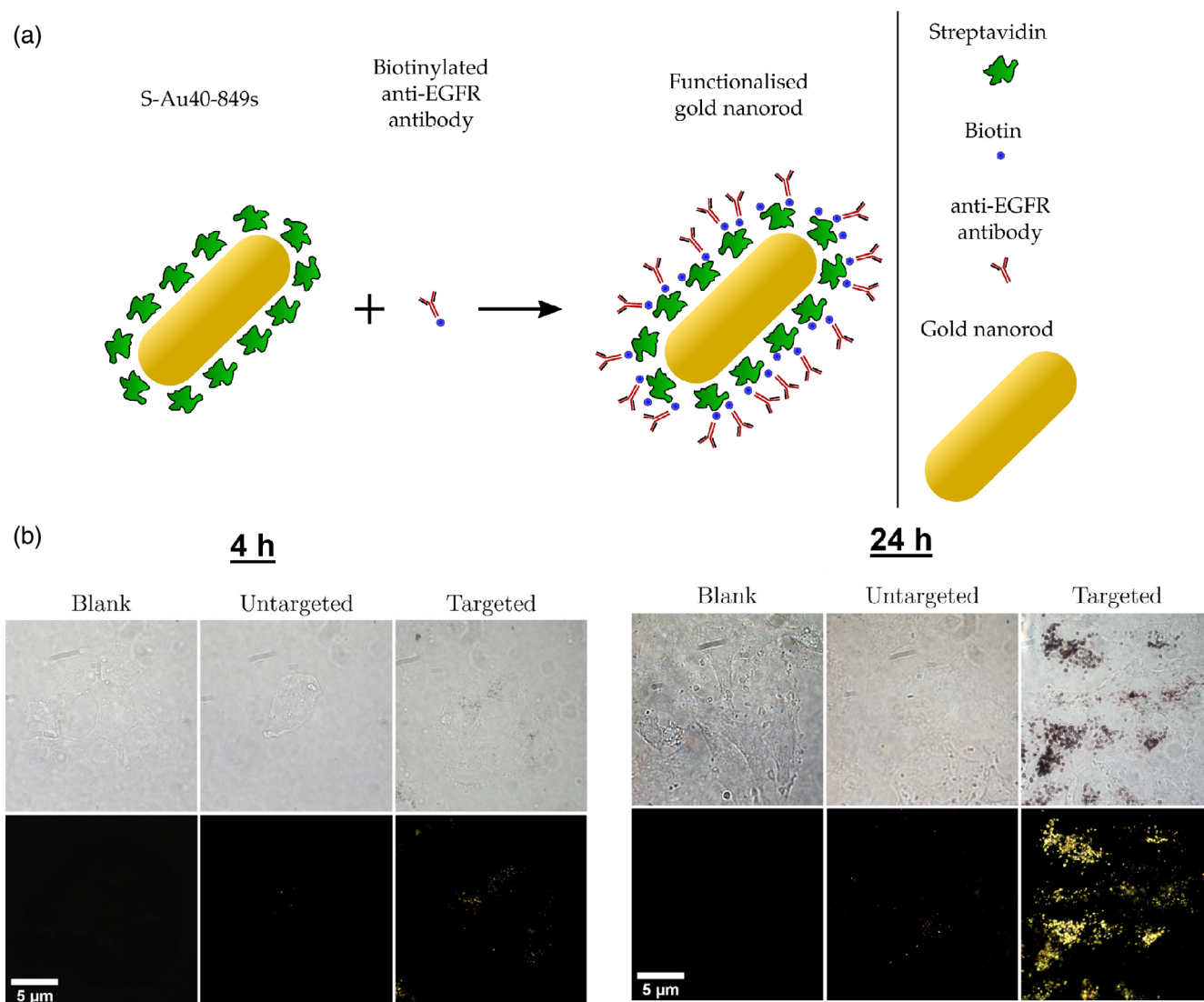


FIGURE 3 Targeted versus untargeted gold nanorods. (a) Schematic of gold nanorods functionalized with biotinylated anti-epidermal growth factor receptor (anti-EGFR) antibodies demonstrate selective cellular uptake using (b) bright field and dark field images of A549 lung cancer cells at incubation times of 4 h and 24 h compared to untargeted gold nanorods (Knights et al., 2020).

could further investigate this combination strategy in addition to delivering the laser light interstitially to potentially enhancing the current LITT procedure.

Another unique type of inorganic nanoparticle used for hyperthermia treatment is *magnetic iron oxide nanoparticles*. NanoTherm[®] is the first nanotechnology-based therapy approved by the European Medicines Agency for treating brain tumors (NCT05010759). These nanoparticles are approximately 15 nm in diameter; however, they can also range from 1 to 100 nm. The earlier work with magnetic iron oxide nanoparticles were for directing drug distribution in the body using a magnetic field (Tong et al., 2019). This approach has expanded to include the use of lasers and MRI for localized hyperthermia treatment (Mahmoudi et al., 2018; Revia & Zhang, 2016). Heat generation is achieved via hysteresis losses by applying an alternating magnetic field (Tong et al., 2019). More recently, magnetic iron oxide nanoparticles along with gold nanoparticles have been described for potentially assisting laser ablation. Ashikbayeva et al. developed a high-scattering nanoparticle-doped fiber for obtaining, in real-time, an accurate superficial thermal map in addition to mediating laser ablation with and without nanoparticles (Ashikbayeva et al., 2020). However, this ex vivo study did not test the nanoparticle system using an interstitially delivered laser setup. Therefore, future studies using magnetic iron oxide nanoparticles with laser activation will require in vivo studies to carefully characterize thermal injury of tissues. Section 4.4 will cover thermal sensing applications in more detail, as well as other types of inorganic nanoparticles such as metal-ion-cross-linked tannic acid (MITA) coordinated onto polymeric and mesoporous silicon dioxide-based nanoparticles (FeIII, VIII, and RuIII) and radiolabelled copper nanoparticles (Cui et al., 2018; T. Liu et al., 2018).

More recently, *magnesium nanoparticles* (Mg nanoparticles) have been reported to be a promising alternative to the frequently studied silver, gold, and copper nanoparticles while maintaining localized surface plasmon resonance properties (Biggins et al., 2018; J. Zhang et al., 2014). Colloidal Mg can be synthesized using a Mg organometallic precursor (e.g., di-*n*-butyl magnesium or bis(cyclopentadienyl) magnesium [Cp₂Mg]) mixed with the reducing agent lithium naphthalide under an argon atmosphere. The Mg nanocrystals undergo nucleation and growth from the reduction of the organometallic precursor, which then produces single-crystalline hexagonal Mg nanoparticles that can range from 100 to 300 nm in size (measured from tip to tip) (Biggins et al., 2018; Jeon et al., 2011). For example, a study in 2014 utilized Mg nanoparticles in silico to illustrate their unique properties and their ability to enhance LITT by improving laser heating efficiency and conformality. These can degrade into absorbable magnesium ions and offer a more biocompatible alternative approach that could work synergistically with interstitial laser light delivery. Mg nanoparticles with a size of 80 nm were delivered to liver tumors in conjunction with thermal therapy in a theoretical simulation and conceptual experiment done by Zhang et al. It was discovered that thermal heating efficiency can be improved up to 20% compared to a system without nanoparticles and a system saturated with nanoparticles (J. Zhang et al., 2014). In addition to improved heating efficiency, the addition of Mg nanoparticles with a multi-beam showed promise in improving LITT's conformal ablation regions. However, more quantitative studies comparing this approach to other nanoparticle-assisted LITT systems are needed.

2.2 | Organic nanoparticles

In contrast to inorganic nanoparticles, organic nanoparticles are biodegradable and therefore could be less toxic. They offer an exciting alternative to using gold nanoparticles to enhance LITT, as well as having opportunities to form dual-combination organic-inorganic nanoparticles by leveraging gold nanoparticles with temperature-sensitive liposomes to achieve controlled drug release. Porphysomes and temperature-sensitive liposomes loaded with gold nanoparticles are the main types of organic nanoparticles that have been recently reported in the literature for interstitial laser therapy.

Porphysome nanovesicles were first described by Lovell et al. in 2011, who showed that these particles could passively accumulate in tumors and actively or passively be loaded with drugs in the aqueous core similar to liposomes. Porphysomes are formed via supramolecular self-assembly of porphyrin-lipid building blocks, which are highly fluorescent (Lovell et al., 2011; Muhanna et al., 2015). When self-assembled, the numerous porphyrin-lipids are tightly packed, resulting in highly absorptive nanoparticles that are fluorescent-silent and can efficiently convert laser light energy to heat energy for photothermal therapy and photoacoustic imaging (PAI). These characteristics are typically not seen with organic nanoparticles, especially noting the fact that their optical extinction coefficients (10^8 – $10^{10} \text{ M}^{-1} \text{ cm}^{-1}$) are like gold nanoparticles which enable porphysomes to generate comparative thermal dosing (Huynh & Zheng, 2014; Jin et al., 2016; Tang et al., 2018). A recent study by Muhanna et al. demonstrated that porphysome nanoparticles could be used for detection and treatment of head and neck cancer in both buccal mucosa

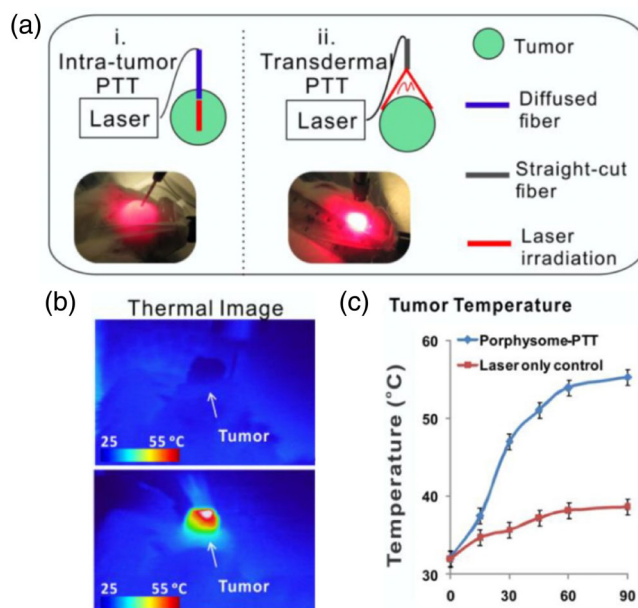


FIGURE 4 Porphysome nanoparticles enable two-step intratumor and transdermal photothermal therapy. (a) Experiment flow demonstrating how porphysome nanoparticles enable two-step intratumor and transdermal photothermal therapy, as well as (b) thermal images displaying temperature profile of hamster oral carcinoma model before (0 s) and after (100 s) of laser irradiation. (c) Tumor temperature plot from the thermal images for each group ($n = 3$) with calculated mean and SD (Muhanna et al., 2015).

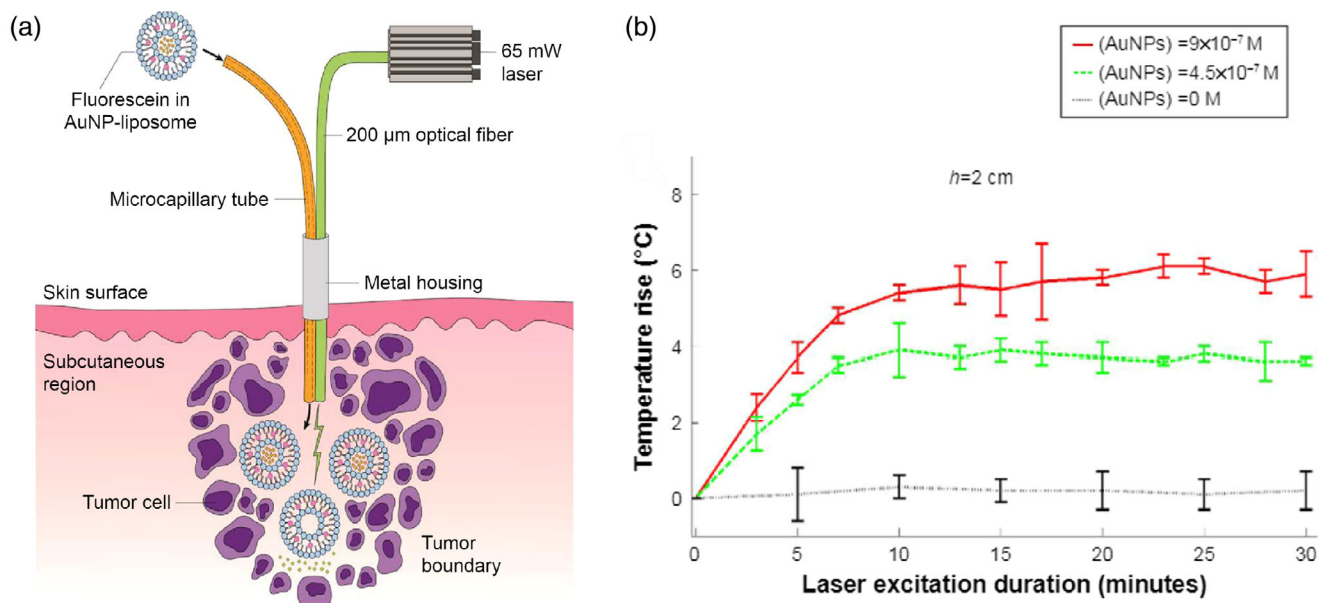


FIGURE 5 Thermosensitive liposome formulation for controlled release of fluorescein. (a) Concept schematic of co-delivered interstitial fiber optic cable and gold nanoparticle-liposomes loaded with fluorescein to trigger controlled release of fluorescein. (b) Ex vivo temperature profiles (mean \pm SD, $n = 3$) demonstrate the dependence of both gold nanoparticle concentrations and excitation durations (H. L. Huang et al., 2015).

squamous cell carcinoma rabbit model and hamster check carcinogenesis model. The synthesized porphysomes were reported to be 117.8 ± 2.0 nm in size and passively accumulated to tumor cells leading to gradual nanostructure dissociation within the interstitial tumor space. The dissociated porphyrin-lipids enable fluorescent imaging to potentially aid in improved treatment specificity and surgeries. The remaining porphysome nanoparticles that have not been dissociated enable PAI and two-step intratumor and transdermal photothermal therapy (Figure 4a) (Muhanna et al., 2015).

Tumor temperature increased from an initial 32.00 ± 0.17 to $55.30 \pm 0.22^\circ\text{C}$ within 90 s of interstitial laser light delivery and external laser irradiation (Figure 4b) (Muhanna et al., 2015).

A *dual-combination inorganic and organic nanoparticle* formulation approach for controlled drug delivery and release has been demonstrated with interstitial laser light delivery via a fiber optic cable to treat breast cancer (Figure 5a) (H. L. Huang et al., 2015). These liposomes encapsulated fluorescein as a surrogate for simulating drug content release profiles. Liposomes are a very effective organic nanoparticle for drug delivery in several approved and ongoing clinical applications [Doxil[®] (Barenholz, 2012), VYXEOS[™] (Lancet et al., 2021), Onivyde[™] (H. Zhang, 2016), and CombiPlex[®] (Tolcher & Mayer, 2018)]. In this study, hydrodynamic size reported for each component was 5.55 ± 2.1 nm for gold nanoparticles and 91.28 ± 12.1 nm for liposome-gold nanoparticles. Initial ex vivo results demonstrated that the photothermal conversion efficiency of gold nanoparticles embedded liposomes is proportional to gold nanoparticles concentration and excitation duration resulting in relatively insignificant temperature rise ($0.2 \pm 0.51^\circ\text{C}$) without gold nanoparticles and 3.9 ± 0.15 or $5.9 \pm 0.63^\circ\text{C}$ with gold nanoparticle concentrations at 4.5×10^{-7} or 9×10^{-7} M (Figure 5b), respectively. In vitro results demonstrated that the combination of 33 ng ml^{-1} of gold nanoparticles embedded to liposome membrane resulted in a significantly higher permeability and more efficient fluorescein release ($74.53 \pm 1.63\%$) compared to liposomes without gold nanoparticles ($14.53 \pm 3.17\%$) within a 40-min time frame with light. Additional in vivo results from mouse models demonstrated that liposomes with gold nanoparticles and 75 mM fluorescein encapsulated nanoparticle had an immediate fluorescence intensity spike compared to no light activation of the same nanoparticles. Specifically, for chemotherapy, long lasting and targeting content release characteristic of liposomal vesicles can result in a higher concentration of the cytotoxic drug in the tumor while also preventing the drug from being exposed to unwanted tissue. In combination with an interstitially delivered laser light source, liposomes overcome the limitations of light penetration depth and issues with uniform drug delivery within the tumor region.

3 | TYPES OF MODELS TO STUDY THERMAL AND BIOLOGICAL IMPACTS

Mathematical modeling and simulation studies have played a major role in advancing the field of nanoparticle-assisted LITT. Most of the work in the past two years has been performed using numerical predictive modeling to better understand the heating profiles of nanoparticles embedded in tissues to improve LITT. Several groups have also demonstrated that these models could be translated into phantoms and animal organs (Ashikbayeva et al., 2020; Chongsathidkiet et al., 2018; Elliott et al., 2010; Xu et al., 2011). In more recent years, translation from mathematical and phantom models to animal studies, including mice, rabbits, guinea pigs, and canines, have been reported with positive results (Muhanna et al., 2015; Schwartz et al., 2009). In addition, the combination of mathematical modeling and in vitro studies can also be beneficial for studying light activation of nanoparticles in a small-scale cancer cell system (Dickerson et al., 2008; H. C. Huang et al., 2009, 2010; Z. Qin & Bischof, 2012). The emerging field of nanoparticle-assisted LITT leverages interstitially delivered fiber optic cables to overcome limitations such as light penetration depth and laser light selectivity. All these advancements and approaches create exciting opportunities that can lead to a truly selective LITT system such that functionalized nanoparticles will primarily target tumors to enable controlled temperature change for achieving minimal to no normal tissue damage. For example, a company called Nanospectra[™] is leveraging gold nanoshell-directed interstitial laser therapy to target and treat prostate cancer. It is currently the first and only ultrafocal tissue ablation therapy technology undergoing clinical trials (Rastinehad et al., 2019; Schwartz et al., 2011; Stern et al., 2016). The following section summarizes commonly used modeling approaches and its translational aspect to in vivo work with a focus on nanoparticle-assisted LITT and its biological impacts.

3.1 | Computational methods and modeling approaches

An effective way to study laser–tissue interaction, nanoparticle–laser interaction, temperature distribution, and thermal damage is the application of computational methods and simulations. Traditional modeling includes three main approaches: (i) using different optical models to calculate laser energy distribution, (ii) using Penne's bioheat transfer equation to calculate temperature changes, and (iii) using Arrhenius damage law to calculate the extent of thermal damage (Kannadorai & Liu, 2013). There are multiple optical modeling equations that can be employed to simulate light interaction in biological tissues at the macroscale. A few that are summarized and reported in the literature

include the radiative heat transfer equation (RTE) (Bayazitoglu et al. 2013; Vera & Bayazitoglu, 2008), Monte-Carlo method (Germer et al., 1998; Wang et al., 2010; Yaroslavsky et al., 2002), and P1 approximation and variations (Bayazitoglu et al., 2013; Elliott et al., 2009). Each of these methods has their own advantages and limitations (Bayazitoglu et al., 2013; Z. Qin & Bischof, 2012). RTE and statistical-based Monte-Carlo method are two of the more commonly reported approaches for studying nanoparticle-assisted LITT. RTE contains space and direction coordinates, local absorption and scattering coefficients, and scattering phase function to relate optical property changes when nanoparticles are introduced to the tissue environment (Bayazitoglu et al., 2013). However, RTE is much more difficult to solve directly and requires additional functions to calculate the scattering phase function, such as Henyey–Greenstein function. The Monte-Carlo method simulates a “random walk,” which relates to the scattering and absorption of photons in the tissue. This method is reported to be easy to implement to solve complex geometries but computationally expensive because of its requirement for enough photons to be launched and traced for it to be accurate (Z. Qin & Bischof, 2012).

In 2010, Wang et al. reported developing a Monte-Carlo method with the Pennes bioheat transfer equation to simulate gold nanoshell-enhanced LITT in a liver tumor model surrounded by normal tissue. This model characterized the cooling effect, also called the heat sink effect, based on blood flow surrounding the tumor region and the gold nanoshell's impact on the immediate microenvironment from the laser activation. The Monte-Carlo method accounted for the absorption coefficient, the scattering coefficient, and the anisotropic factor to accurately quantify the effects of adding gold nanoshells to the medium and to effectively simulate optical property variations in tissues during LITT. Laser power of 3 W was used for all comparison studies up to 100 s. Optimal gold nanoshell sizes of R55/80 and R40/80 (e.g., core radius [40]/core [40] + gold shell radius [40]) and concentration ($1 \times 10^{10} \text{ ml}^{-1}$) were reported from testing various sizes including R40/45, R50/60, R40/55, R55/80, R40/80, and R75/115 and concentrations ranging between 1×10^9 and $1 \times 10^{11} \text{ ml}^{-1}$ (Wang et al., 2010).

Another study by Kannadorai and Liu aimed at developing a model to effectively optimize parameters for the treatment of differently sized spherical tumors using interstitial plasmonic photothermal therapy with gold nanorods (Kannadorai & Liu, 2013). The standard Pennes bioheat equation and the Arrhenius damage law were used to determine the distributions of temperature and thermal damage within the simulated tissue model, respectively. Then, a suitable optimization algorithm was developed in conjunction with these equations to achieve complete spherical tumor destruction plus an additional 1-mm normal tissue damage. Previous models considered each of the parameters (laser power density, gold nanoparticle concentrations, and exposure time) individually. In contrast, this study considered all three in a single objective function with each parameter assigned its respective weights (Ashikbayeva et al., 2020; Vera & Bayazitoglu, 2008; Wang et al., 2010; Yin et al., 2020; J. Zhang et al., 2014). For each tumor size (radii of 2, 3, 4, and 5 mm), a total of 125 different weight sets were evaluated for all three parameters. Results from this study confirmed the importance of optimizing gold nanorod concentrations. Varied concentrations of 2.5×10^9 , 5.0×10^9 , 7.5×10^9 , and 10.0×10^9 nanoparticles ml^{-1} that was embedded in a 5-mm radius spherical tumor and activated by a laser with $3.0 \times 10^3 \text{ W m}^{-3}$ showed that increasing nanorod concentration reduced temperature distribution due to the nanoparticle's strong light absorption as well as containing thermal energy within the nanoparticle delivered region (Kannadorai & Liu, 2013).

The main types of nanoparticles that have been studied in these models are gold nanoshells and gold nanorods due to their clinical relevance. Another proposed alternative nanoparticle with clinical potential is Mg nanoparticles (J. Zhang et al., 2014). In addition, a combination of parameters, including nanoparticle size, nanoparticle concentration, direct injection versus intravenous injection, single- versus multi-beam laser delivery, laser power, and laser exposure times, should all be taken into consideration and studied exhaustively to better understand laser–tissue interactions and temperature affects within the simulated system. Conclusions from these reported models demonstrated that nanoparticle-assisted LITT can effectively reduce undesirable damage to healthy tissues, improve controlled heat distribution, and reduce laser exposure time.

3.2 | Combinations of phantom gels, ex vivo, and in vitro models

Tissue mimicking materials, such as phantoms, have been studied extensively to achieve optical and physical properties comparable to the tissue or the tumor of interest. Phantom material make-up and properties can range from simple to complex depending on what type of tissue is being mimicked (D'Souza et al., 2001; Haj-Hosseini et al., 2014; S. Liu, Doughty, et al., 2018). Previous studies have used phantoms in combination with numerical modeling to study

nanoparticle-assisted LITT in the liver, prostate, and brain cancer (Assi et al., 2021; Elliott et al., 2010; S. Liu, Doughty, et al., 2018). It is important to consider the optical properties of the target and nontarget tissues when developing and using phantoms for studying laser applications, especially for nanoparticle-assisted LITT. For example, foundational work reported by numerous groups have set the precedence for the importance of tissue and nanoparticle optical properties in relation to photon absorption by tissue chromophores, irradiation parameters, spatial temperature profiles, and thermal affects (Gebhart et al., 2006; Schwarzmaier et al., 2002; Stewart et al., 2017; Yaroslavsky et al., 2002).

The most extensively researched system, gold nanoparticle-enhanced photothermal treatment, has great potential to enhancing LITT because of its ability to increase thermal conductance and capacitance within the tumor while decreasing heat transfer to surrounding normal tissues (Ali et al., 2017; Dickerson et al., 2008; Z. Qin & Bischof, 2012). An example of this is shown in a study by Huang et al. that used mathematical modeling of gold nanorods dispersed in an in vitro human prostate cancer cell monolayer system to characterize the spatiotemporal changes of temperature upon NIR laser irradiation. The laser was set to 800 nm with a 2-mm diameter diffuser and a fixed laser power density of 20 W cm^{-2} for 15 min. This work demonstrated that gold nanorods dispersed in the extracellular space can also be an effective method of inducing cancer cell death as compared with earlier work focused on intracellular hyperthermia (H. C. Huang et al., 2010). Future studies should also consider this parameter and the previously mentioned parameters (laser power density, gold nanoparticles concentration, and exposure time) that can be studied with these models.

Elliott et al. reported the use of gold nanoshells to assist and enhance LITT in a simulated 3D finite element modeling approach which was then applied to agar gel phantoms to mimic canine liver tissues (Elliott et al., 2010). The laser wavelength range was between 790 and 830 nm to deliver a laser power of 15 W via a 2-mm diameter catheter with an irradiation time of 300 s. The optical properties of the developed phantom were based on previously measured optical properties of liver and tumor (Germer et al., 1998). Optical properties were reported (Figure 6a) to change dramatically before and after the addition of gold nanoshells, which included an overall increase in the scattering coefficient ($10.8\text{--}57.4 \text{ cm}^{-1}$), absorption coefficient ($0.6\text{--}2.89 \text{ cm}^{-1}$), and optical penetration depth ($0.6\text{--}0.12 \text{ cm}$), respectively (Elliott et al., 2010). A liver phantom and tumor phantom were then developed based on these measurements and then combined afterward to mimic a tumor within healthy liver tissue (Figure 6b) (Elliott et al., 2010). The ex vivo phantom contained a general liver phantom combined with a tumor phantom distributed with and without gold nanoshells. The laser fiber was inserted directly into the phantom tumor center and heating profiles using real-time MR temperature imaging, also commonly known as MR thermometry (Figure 6c) (Elliott et al., 2010). Both models indicated that higher concentrations of gold nanoshells intravenously delivered to a solid liver tumor will likely result in higher accumulation

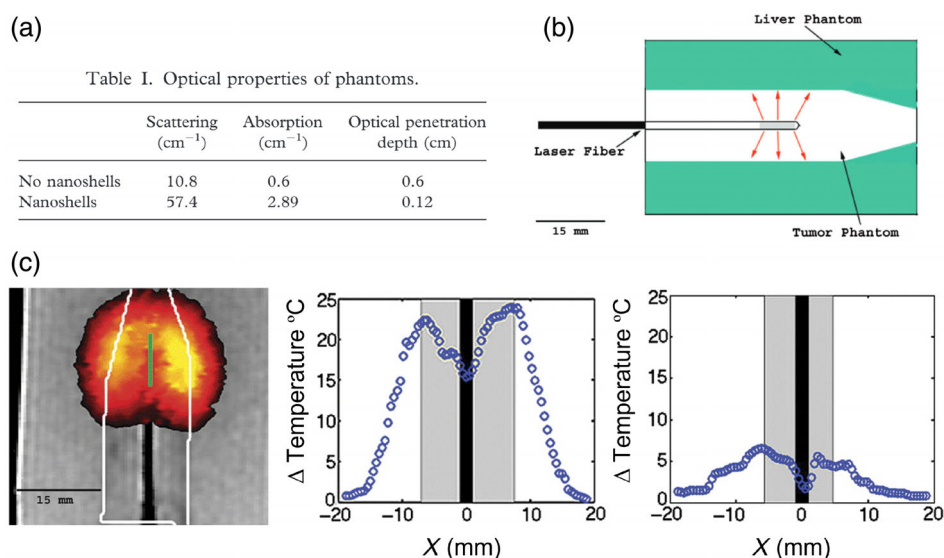


FIGURE 6 Interstitial fiber optic cable delivery in a tumor and liver phantom containing gold nanoshells. (a) Table summarizing changes in optical properties of liver phantoms before and after addition of gold nanoshells. (b) Schematic drawing of experimental set up to demonstrate interstitial fiber optic cable delivery of tumor and liver phantoms. (c) Magnetic resonance thermal image (MRTI) displaying thermal distribution of gold nanoshells in the tumor. Temperature profiles comparing maximum temperature changes with gold nanoshells and without gold nanoshells (Elliott et al., 2010)

within the tumor tissues, which resulted in improved heating confined within the lesion (Figure 6d) (Elliott et al., 2010).

In the same study by Elliott et al. (2010), animal organ models were developed using canine liver containing a tumor phantom to study the effects of nanoparticle-assisted LITT compared to LITT alone. Results from the phantom and canine liver experiments demonstrated that higher gold nanoshell accumulation in the tumor regions offer the advantage of enhancing heating when combined with LITT. By using MR thermometry, maximum temperature changes were measured in phantoms in the presence (24°C) and absence of gold nanoshells (6°C) (Elliott et al., 2010). Later, the same group used an alternative approach to studying *in vivo* gold nanoshell accumulation and local optical property variations from thermal images collected during a previous nanoparticle-mediated, MRI-guided LITT study in canines. An algorithm was developed using a statistical inverse problem formulation with a finite element method to estimate the optical parameters based on the thermal images. The model developed can potentially be used to correlate the distribution of nanoparticles *in vivo* to MR temperature imaging with and without nanoparticles. Porcine livers and pork loin tissues have also been reported as models to study the effects of heat from laser light activation of embedded nanoparticles (Ashikbayeva et al., 2020; Assi et al., 2021). These studies focused primarily on demonstrating alternative approaches to real-time temperature monitoring to mediate laser ablation in tissues which will be discussed in the next sections.

Based on mathematical modeling, phantom gels, and *ex vivo* animal organ models higher gold concentrations result in higher absorption of light energy and higher heating in specific areas where nanoparticle activation is located leading to reduced tissue injury in the surrounding normal tissue. However, continued laser irradiation and an increase in nanoparticle concentration above a certain threshold will cause minor hyperthermia (Bayazitoglu et al., 2013). Studies emphasize the need to optimize different systems with varying ranges of gold nanoparticles concentration, laser power, and irradiation times. This is attributed to the shift optical properties of tumors and their surrounding tissues undergo from pretreatment to when nanoparticles are introduced and during nanoparticle-assisted LITT treatment (Elliott et al., 2010; J. Zhang et al., 2014). Our summary of nanoparticle-assisted LITT indicates that the following parameters and their ranges have been reported to achieve cell death *in vitro* and *in vivo* models: laser power (0.7–5 W) with irradiation times ranging from 100 to 600 s (Muhanna et al., 2015; Stern et al., 2016; J. Zhang et al., 2014), gold nanoshell concentrations ranging from 5.6×10^8 to $1 \times 10^{10} \text{ ml}^{-1}$ (Schwartz et al., 2011; Wang et al., 2010; Zharov et al., 2005), and gold nanorod concentrations ranging from 2.5×10^9 to $1 \times 10^{10} \text{ ml}^{-1}$ (Kannadorai & Liu, 2013). Translation from numerical modeling and theoretical simulations to nanoparticle embedded tissue phantoms and animal organs are essential models that can be studied in parallel with *in vitro* modeling, which presents an advantageous strategy before moving into *in vivo* models and ultimately translation to the clinic.

3.3 | *In vivo* models and biodistribution

Current research into the toxic effects of nanoparticle and interstitial laser light delivery *in vivo* has not been extensively reported. A few recent studies have looked into these effects and compared LITT alone with nanoparticle-assisted LITT, which will be discussed further below. A summary of the collected work (Figure 7) shows the varying laser powers that are tested and required for achieving nanoparticle-assisted interstitial hyperthermia or nanoparticle activation for controlled drug delivery as compared to current clinical LITT systems (Ashikbayeva et al., 2020; Elliott et al., 2010; Fuentes et al., 2013; H. L. Huang et al., 2015; Kamath et al., 2017; Muhanna et al., 2015; P. Patel et al., 2016; Schwartz et al., 2009, 2011; Stern et al., 2016; Wang et al., 2010; Xu et al., 2011; J. Zhang et al., 2014). The laser power needed averages below 5 W as further summarized in more detail in Table 1, which has minimal effect on surrounding tissue and is advantageous for selective interstitial hyperthermia tumor treatments. In addition, promising translational work in gold nanoshell (Auroshells™) assisted interstitial PTT by Nanospectra™ as well as work that focuses on developing tools for studying temperature at the nanoscale level will potentially aid in moving this field forward (Gad et al., 2012; Hastman et al., 2020; Rastinehad et al., 2019; Stern et al., 2016).

In 2009, Schwartz et al. (2009) reported feasibility studies of nanoparticle-assisted LITT using orthotopic canine models of brain cancer. Interstitial fiber optic delivery of NIR light with a wavelength of 808 nm and laser dosing of 3 min was used for activation of 150-nm gold nanoshells that had accumulated in the intracranial tumors. Hematoxylin and eosin staining, MRI, and elemental analysis were used to track changes in thermal coagulation, controlled heating, and nanoparticle distribution, respectively. This approach demonstrated a selectively elevated temperature increase in the tumor tissue to $65.8 \pm 4.1^\circ\text{C}$ compared to the normal white and gray matter tissues, which

Nanoparticle-assisted LITT versus MRI-guided LITT trend

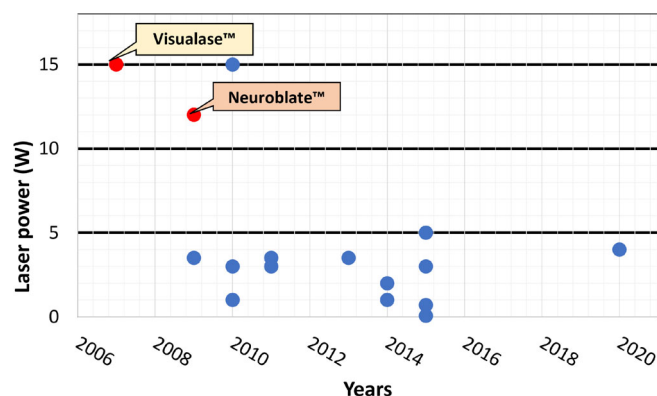


FIGURE 7 Nanoparticle-assisted laser interstitial thermal therapy (LITT) versus magnetic resonance imaging (MRI)-guided LITT trend. Summary of varying laser powers tested and required for achieving nanoparticle-assisted interstitial hyperthermia or nanoparticle activation for controlled drug delivery compared to current clinical LITT systems. Required laser power averages below 5 W (Ashikbayeva et al., 2020; Elliott et al., 2010; Fuentes et al., 2013; H. L. Huang et al., 2015; Kamath et al., 2017; Muhanna et al., 2015; P. Patel et al., 2016; Schwartz et al., 2011, 2009; Stern et al., 2016; Wang et al., 2010; Xu et al., 2011; J. Zhang et al., 2014)

demonstrated a sublethal temperature increase of $48.6 \pm 1.1^\circ\text{C}$. Thus, the combination of gold nanoshells with LITT displayed an overall lower temperature increase in normal tissues compared to tumor targeted regions (Schwartz et al., 2009). A recent study by Bagley et al. reported an alternative method to the traditional direct insertion of fiber optic cables to the tumor region (Bagley et al., 2013). This study aimed at overcoming current limitations in adequately delivering NIR light for PTT by implanting a NIR device composed of a silica rod and flexible mesh in combination with PEGylated gold nanorods to treat intraperitoneal ovarian tumors. A combination of computational and in vivo models were used to select top candidate devices and implant them to an orthotopic ovarian cancer model using OVCAR8 human ovarian cancer cells expressing firefly luciferase. Temperature increases were able to be contained within the tumor region due to the accumulation of the gold nanorods. Histological staining was also performed on the tissues following thermal therapy with the NIR devices revealing thermal damage at the tumor site while not inducing irreversible damage to other organs (Bagley et al., 2013).

In a different study, Lovell et al. investigated a high dose of intravenously delivered porphyrins (1000 mg kg^{-1}) to xenografted nude mice inoculated with KB cells (human epidermoid carcinoma cells) and reported that they remained healthy with no major behavioral changes or weight loss over a 2-week period (Lovell et al., 2011). More recently, this organic nanoparticle has also been introduced as a potential agent for combination phototheranostic and targeted head and neck cancer (Muhanna et al., 2015). Specifically, by applying a two-step photothermal therapy approach, the ablation of head and neck tumors was studied in male Syrian hamsters and New Zealand white rabbits. In this study, biodistribution and pharmacokinetics were mainly studied in the hamster model in addition to histology analysis to assist in investigating porphyrin accumulation at the cellular level. Porphyrins were systemically administered, and organs of interest were dissected and homogenized after 24-h postnanoparticle delivery. The dissected organs included tumors, healthy mucosa, heart, kidney, spleen, small intestine, large intestine, and hind limb muscle. Biodistribution analysis was based on the fluorescence signal from porphyrin. Results showed an average accumulation of $3.85\% \text{ ID g}^{-1}$ (% of injected dose per gram of tissue) in the tumor compared to only $0.29\% \text{ ID g}^{-1}$ in the healthy oral mucosa. This result demonstrates an effective co-localization of porphyrin nanoparticles within the tumor environment while also being efficiently circulated out of the body in higher % ID g^{-1} in organs such as the liver, spleen, and small intestine (Muhanna et al., 2015).

Additional posttreatment evaluation of porphyrins in rabbits were also conducted and tracked at three different time points (preinjection, 24-h postinjection, and 4 weeks postinjection-PTT). Specifically, blood panel assay and hematoxylin and eosin staining of sectioned organs were performed to better understand porphyrins' biological safety and biocompatibility via systemic administration. Alkaline phosphatase was the only marker reported to decrease at the 4-week time point; however it was still within normal ranges. Other levels at each time point were all within range and did not exhibit any significant changes which included alanine transaminase, amylase, blood urea nitrogen, creatinine, white blood cell, red blood cell, hemoglobin, and hematocrit (Muhanna et al., 2015).

TABLE 1 Summary of studies investigating delivery of nanoparticles in combination with interstitially delivered laser light for cancer treatment (T = temperature)

Author	Nanoparticle	Model details	Light	Max T reported	Imaging/sensing modality	Outcomes
Ashikbayeva et al. (2020)	Gold nanospheres, 20 nm Magnetic iron oxide, 20 nm	Ex vivo porcine liver tissue	Fiber-coupled mid-power laser (400 μ m, 980 nm, 4 W, 144 and 140 s)	111.6°C/162.39°C	Optical backscattering reflectometry (OBR) fiber-coupled laser diode Nanoparticle-doped optical fibers	Nanoparticle-doped sensors displayed precision sensing and accuracy Addition of nanoparticles to tissue increased ablation area
Yin et al. (2020)	Gold nanospheres, 30 nm	In silico 2D axisymmetric model of biological tissues with a spherical tumor	Not specified (630 nm; 0.1, 0.01, and 0.05 W mm ⁻² ; 70–390 s)	80–120°C	N/A	Addition of gold nanoparticles increased laser energy absorption and increased temperature
Vera and Bayazitoglu (2008)	Gold nanoshells, 42 nm	In silico various (human brain, breast, subcutaneous fat, liver, and skin)	Helium–neon laser delivered by a fiber optic cable (633 nm; 5000, 10,000, 15,000, and 20,000 W m ⁻² ; 260–557 s)	55°C	N/A	Addition of nanoshell significantly reduced time to reach maximum temperatures compared to tissues without nanoshells; however, too many nanoshells cause undesirable temperature differential
Wang et al. (2010)	Gold nanoshells, (core radius/gold shell radius) R40/45, R50/60, R40/55, R55/80, R40/80, R75/115	In silico normal and metastatic human liver tissue	Not specified (830 nm, 3 W, 90 s)	71.4°C	N/A	Increased particle size led to increased temperature. But increased concentration led to increased T , then decreased T . Addition of particles reduced thermal damage to healthy surrounding tissue from 5 to 2.5 mm
Xu et al. (2011)	Gold nanoshells, R40/110 Gold nanorods	In silico various cylindrical tumor phantom (prostate, breast, brain)	Diode laser (cylindrical diffusion applicator, 20 mm length \times 1 mm radius, 850 nm, and 633 nm, 1 W, 30/60/90 s)	59°C	N/A	Addition of high-preferential absorbance properties enhances local transduction of photon energy to thermal energy and shorter heating period for desired temperatures
Kannadorai and Liu (2013)	Gold nanorods, 38 nm \times 10 nm	In silico spherical tumors: series of radii including 2, 3, 4, and 5 mm	Near-infrared laser light (1 mm \times 2R + 2 mm; R = 2, 3, 4, 5 mm, 785 nm; 0 to 3 \times 10 ³ W m ⁻³ , 900 s)	72.5°C	N/A	Increase in nanorod concentration results in decrease thermal damage depth

(Continues)

TABLE 1 (Continued)

Author	Nanoparticle	Model details	Light	Max <i>T</i> reported	Imaging/sensing modality	Outcomes
Elliott et al. (2010)	Gold nanoshells, R55/60	In silico and ex vivo canine liver tissue and agarose gel phantoms	Diode laser (808 nm, 15 W, 300 s)	Max change in <i>T</i> = 45°C	MRTI	Average discrepancy was 1.6°C, maximum difference between in silico model predictions and ex vivo was 3.8°C
J. Zhang et al. (2014))	Magnesium, 80 nm	In silico and ex vivo porcine liver tissue	Near-infrared laser and two-diode laser (1 mm, 850 nm, 5 W and 808 nm, 1 W or 2 W, 300 or 60 s)	Cubic liver up to 90°C Irregular liver up to 80°C Ex vivo up to 60°C	Thermocouple detectors	Addition of nanoparticles resulted in temperature stability to occur by 10 s compared to no Mg nanoparticles (until after 40 s) and multibeam covered 10X more volume of heating compared to single beam
Bagley et al. (2013))	Gold nanorods, 41 nm × 10 nm	In silico and in vivo orthotopic ovarian tumors by intraperitoneal injection of OVCAR8 cells in female NCR nude mice	Diode laser source (Visotek) through an SMA-threaded glass fiber optic cable (0–4 cm, 810 nm, $4 \times 10^3 \text{ W m}^{-2}$ to $2 \times 10^{-1} \text{ W m}^{-2}$, 30 min)	6.27 ± 2.47°C	CT K-type fiberglass thermocouple	Maximum tumor temperature reached 6.27 ± 2.47°C without permanent tissue damage to enhance delivery of agents
Schwartz et al. (2011))	Gold nanoshells, 150 nm	In vivo canine prostate cancer	15 W gallium arsenide diode laser (400-mm core optical fiber terminated with a 1 cm length of isotropic diffuser, 810 nm, 3 W or 3.5 W, 120 or 180 s)	Not monitored	Not used	Thermal damage is a function of power, not total energy dose (3.5 W yielded more damage than 3 W; 420 J vs. 540 J)
H. L. Huang et al. (2015))	Gold nanoparticle, 5.55 ± 2.1 nm, embedded liposomes, 91.28 ± 12.1 nm	In vivo malignant xenografts (MDA-MB 231 cell/matrigel™) implanted subcutaneously in male nu/nu nude mice	Multi-mode optical fiber-guided diode pumped solid-state laser (200 μm, 532 nm, 0.065 W, 600 s)	5.9 ± 0.63°C	Fluorescence imaging Computed tomography (fluoroscopy)-guided needle insertion	Efficient fluorescein release of 74.53 ± 1.63% compared to no liposomes without gold nanoparticles of 14.53 ± 3.17%
Muhanna et al. (2015))	Porphyosomes, 117.8 ± 2.0 nm	In vivo orthotopic buccal mucosa squamous cell carcinoma rabbit model and hamster cheek carcinogenesis model	Straight-cut fiber (8 mm, 671 nm, 0.7 W, 100 s)	62.33°C	Fluorescence imaging Photoacoustic imaging	Porphyosome and light increased tumor temperature, while light alone minimally increased Blood analysis after 4 weeks of treatment was within normal ranges

TABLE 1 (Continued)

Author	Nanoparticle	Model details	Light	Max <i>T</i> reported	Imaging/sensing modality	Outcomes
Fuentes et al. (2013)	Gold nanoshells, 144–150 nm	In vivo orthotopic transmissible venereal tumor (TVT cells) in canine brain tissue	A catheter for the water-cooled diffusing fiber applicator (400 μ m, 808 nm, 3.5 W, 180 s)	70°C	MRTI	Solution of inverse problem able to reproduce selective heating within 5°C of measured MRTI estimations along selected temperature profile
Schwartz et al. (2009)	Gold nanoshells, 150 nm	In vivo orthotopic transmissible venereal tumor (TVT cells) in canine brain tissue	Diode laser (1-cm-long isotropic diffusing tip, 808 nm, 3.5 W, 180 s)	65.8 \pm 4.1	MRI Thermal mapping	Particles in tumor tissue cause thermal damage, while normal white and gray matter without particles did not
Stern et al. (2016)	Gold nanoshells, silica core, 120 \pm 12 nm Gold shell, 12–15 nm	Clinical Prostate Cancer	Diomed/angiodynamics D15+ laser (400 μ m, 810, 3–5 W, 180–240 s)	N/A	Ultrasound probe Thermocouple	AuroShell™ particles, laser treatment, or prostatectomy did not have adverse effects on blood chemistry analysis

Other areas of development to reduce nanoparticle risk or toxicity effects postinterstitial hyperthermia treatment should still be investigated. Developing biodegradable nanoparticles is one approach that could potentially aid in enhancing LITT treatments. For example, in 2014, the Tsourkas group first reported the development of their dual-combination inorganic and organic gold-loaded polymeric micelles (Al Zaki et al., 2014; McQuade et al., 2015). This work motivated the more recent study demonstrating controlled pH-triggered biodegradable dual-combination inorganic and organic nanocluster formulation. This ~ 150 -nm biodegradable nanocluster consisted of gold nanoparticles (1.7 ± 0.5 nm) that were coated with thiolated dextran modified with acetal groups to make the gold nanoparticles hydrophobic and densely cluster together. This new property of gold allows for it to be loaded to polymeric micelles made of poly(ethylene glycol)₄₀₀₀-*b*-poly(ϵ -caprolactone)₃₀₀₀ (PEG-PCL). Upon exposure to acidic environments, the gold nanoparticles begin to solubilize into smaller components due to the acetal groups being cleaved off, leading to destabilization of the entire nanocluster (Higbee-Dempsey et al., 2020). This approach would not only enable a higher rate of particle removal from the body, but also allow for the release of drugs post-LITT treatment to combat any side effects or to eliminate any untreated cancer cells.

4 | THE ROLE OF NANOPARTICLES TO ADVANCE IMAGING AND THERMAL SENSING

The safety and efficacy of nanoparticle-assisted interstitial thermal therapy is limited by factors that include (i) accumulation and spatial distribution of nanoparticles, (ii) determining the best treatment time, (iii) distribution of generated heat within tumors, and (iv) accurate temperature monitoring. The advancements in engineering multifunctional PTT probes with imaging properties may allow for opportunities to overcome these limitations. Furthermore, various imaging modalities used in combination with nanoparticles as contrast agents have been studied to demonstrate real-time visualization of nanoparticle distribution to optimize treatment effects and real-time temperature monitoring to improve outcomes of image-guided PTT (Quesson et al., 2000; West et al., 2019; Zou et al., 2016). These nanoparticle compositions serve as alternatives to current contrast agents including gold, iron oxide, gadolinium chelates, carbon and manganese-based nanomaterials (Chu et al., 2018; Y Liu et al., 2019; J. Qin et al., 2015). However, it should be noted that most nanomaterials are still at early development stages with a long trajectory toward clinical translation. Various imaging modalities have been studied for interstitial laser delivery, which includes MRI, fluorescence imaging, PAI, positron emission tomography (PET), and computed tomography (CT). MRI remains one of the most commonly used noninvasive techniques for real-time tissue temperature mapping and assessing the extent of ablation (West et al., 2019). However, with the emergence of a nanoparticle-assisted platform for interstitial hyperthermia and nanoparticle-guided imaging modalities, there are great opportunities to minimize collateral damage to healthy tissues and prolong patient survival. The following section will focus on the current limitations of imaging and thermal sensing and how the implementation of nanoparticles in specific clinically relevant and emerging imaging modalities can overcome them.

4.1 | Magnetic resonance imaging

MRI remains one of the most commonly used non-invasive techniques for real-time tissue temperature mapping and assessing the extent of ablation (West et al., 2019). Various MR parameters, including T_1 -relaxation, T_2 -relaxation, diffusion coefficient, and water proton resonant frequency shifts (PRF) are sensitive to thermal changes. Since PRF measurement is relatively independent of tissue type (except adipose tissue), it is the most widely used technique for MR thermal imaging (MRTI) measurements in vivo (De Poorter, 1995). The shifts in tissue water PRF are measured before and after laser treatment followed by analysis via an Arrhenius thermal dose model to generate precise thermal maps with near real-time tissue necrosis visualization. Currently, there are two clinically approved LITT systems that use MRTI technology, Visualase MRI-guided laser ablation by Medtronic and NeuroBlate system by Monteris Medical. While the NeuroBlate system is designed specifically for use within the brain, Visualase is employed for an array of medical areas including neurosurgery, cardiovascular thoracic surgery, head and neck surgery, dermatology, urology, pulmonology, radiology, and more. In addition to providing a soft tissue contrast to identify lesion and confirm the proper positioning of laser probe within the target lesion, MRI allows one to monitor delivery of energy over time, visualize the thermal damage in real time and define temperature check points to enable feedback loop-based control plan tailored to the tissue characteristics.

The incorporation of nanoparticles to improve PTT outcomes has prompted several efforts to develop PTT nanoparticle platforms and algorithms that are synergistic with current MRTI methods. This approach can assist in monitoring the intratumoral spatiotemporal distribution of temperature in real-time, as well as help to estimate the effects of heterogeneous *in vivo* nanoparticle distribution. The latter is achievable due to nanoparticles' optical properties, which can be leveraged as contrast agents to enhance contrast and brightness for MRI. For example, Janus-like magneto-plasmonic hybrid vesicles were prepared by integrating gold and iron oxide nanoparticles in the membrane for strong NIR absorption along with enhanced the transverse relaxation (T2) contrast effect for effective MRI-guided PTT (Y. Liu et al., 2016). This group demonstrated that T2-weight contrast images obtained 2-h after intravenous administration of vesicles into tumor-bearing mice showed 49.3% more darkening from baseline in comparison to 18.6% darkening observed in the absence of a magnet.

In another study, multifunctional doxorubicin-loaded gold nanorod capped magnetic core mesoporous silica shell nanoellipsoids designed by Shi et al. demonstrated synergistic effect of chemotherapy and PTT in one platform while combining the use of MRI and thermal imaging to monitor *in vivo* tumor necrosis (Ma et al., 2012). In another report, Dou et al. fabricated a thermosensitive liposome formulation co-encapsulating cisplatin and the MR contrast agent gadoteridol to allow real-time monitoring of spatiotemporal distribution of nanoparticles, as well as temperature distribution and heat-activated release of the payload in tumor-bearing mice via MRI (Dou et al., 2014). Liu et al. investigated the photothermal potency of a range of MITA coordinated onto polymeric and mesoporous silicon dioxide-based nanoparticles including Fe^{III}, V^{III}, and Ru^{III} (T. Liu et al., 2018). They demonstrated that while these metal ions did not affect the materials' photothermal conversion efficiency, it played an important role in determining the imaging properties. While Fe^{III}TA nanoparticles produced a longitudinal relaxivity coefficient (r_1) of 4.19 mM⁻¹ s⁻¹, Mn^{II} doping enhanced the r_2 value to 71.27 mM⁻¹ s⁻¹) suggesting their use of effective T1- and T2-weighted MRI imaging to estimate the best PTT treatment window after injection.

The use of MRTI to monitor and predict thermal response generated by laser treatment in the presence of nanoparticles has also been widely explored to further optimize the heating and cooling protocols. Stafford and co-workers (Stafford et al., 2011) reported use of feedback MRTI model to estimate the thermal dose from temperature history and monitor the intratumoral spatiotemporal temperature profile in real time during gold nanoshell-mediated thermal ablation in a prostate cancer (PC-3) xenograft model (Figure 8) (Stafford et al., 2011). Their expected MRTI measurements showed a good correlation with temperature maps generated and the associated damage observed in histopathology data. Recently, Fuentes et al. developed high-performance statistical inverse analysis algorithms to estimate the *in vivo* spatial distribution of nanoparticles from the MR thermometry measurements acquired during nanoparticle-mediated LITT procedure (Fuentes et al., 2013). The mathematical model is based on MRTI generated thermal distribution data collected by Schwartz et al. in gold-silica nanoparticle (Auroshells[®])-induced laser ablation of brain tumors in an orthotopic canine model (Schwartz et al., 2009). These data were analyzed using finite element methods of inverse parameter recovery constrained by a Pennes bioheat transfer model to estimate the optical parameters, including optical absorption and thermal conductivity. The determined parameters were used to generate a maximum likelihood solution for estimating the spatial distribution of nanoparticles and predict temperature distribution with respect to the distance from the applicator tip. The results demonstrated good agreement between the predicted and MRTI measured temperatures suggesting potential application in improving nanoparticle-assisted thermal therapy. The developed model, though promising, is currently based on an inferior fluence model and requires additional efforts to improve the accuracy before it can be employed for clinical use.

4.2 | Photoacoustic imaging

PAI has emerged as an alternative high-resolution, deep-penetration, and non-invasive imaging modality that has shown good feasibility with nanoparticle-mediated PTT for both diagnostic and therapeutic monitoring purposes. Various multifunctional nanoplatforms combining PTT and PAI materials have been explored over the years. In a recent study, Phan et al. generated FeOOH@polypyrrole nanorods coated with hyaluronic acid (HA-FeOOH@PPy NRs) for PAI-guided PTT to target CD44-positive breast cancer cells (Phan et al., 2018). The authors observed significant enhancement of PA signal postintratumoral NR injection, providing a detailed structure of tumor region to ensure precise positioning of the external NIR laser. The intratumoral injection of NRs followed by 6-min exposure to NIR laser at a power of 2 W cm⁻² led to the temperature of 62°C resulting in complete tumor eradication 17 days after PTT treatment. In another study, Huang et al. reported design of biodegradable gold nanovesicles (BGVs) where gold

nanoparticles tethered to poly(ethylene glycol)-*b*-poly(ϵ -caprolactone) (PEG-*b*-PCL) showed enhanced plasmonic coupling effect enabling simultaneous PAI imaging and PTT (Figure 9) (P. Huang et al., 2013). The photothermal conversion efficiency of BGVs was observed to be $\sim 37\%$ in comparison to 22% for GNRs.

In addition, PAI has also been explored as a thermometry technique for real-time temperature measurements using a photoacoustic temperature sensing (PATS) system (Meng et al., 2019; Upputuri et al., 2020). PAI uses pulsed laser irradiation of tissue which results in the thermal expansion-relaxation process to induce the generation of acoustic waves. The signal and amplitude depend on the Grüneisen parameter (Γ). The Γ parameter has been demonstrated in

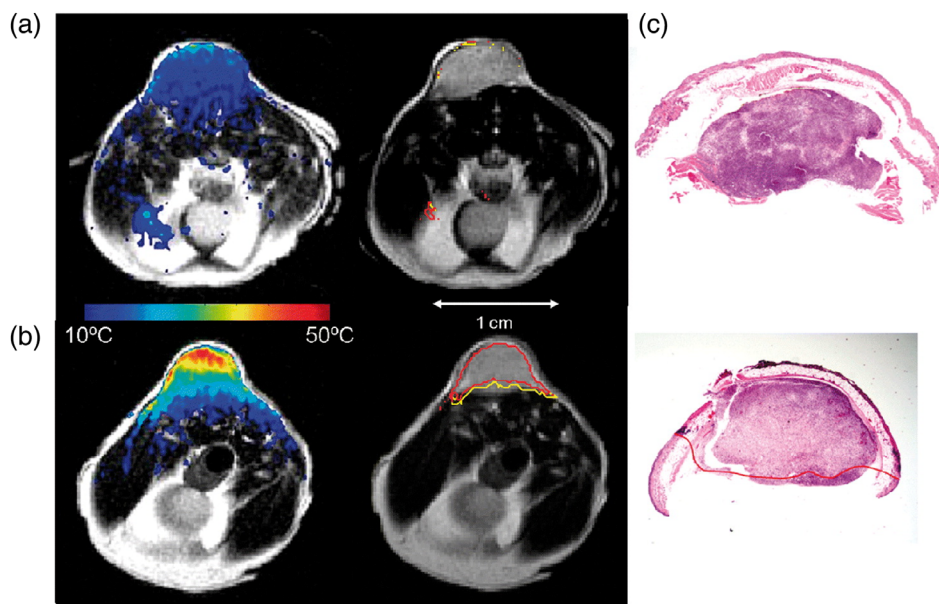


FIGURE 8 Magnetic resonance thermal image (MRTI) images with and without gold nanoshells. MRTI mapped onto T2-W anatomical images of prostate cancer (PC-3) mouse xenografts with calculated maximum temperature change (color scale) where (a) is (–) gold nanoshells compared to (b) (+) gold nanoshells. (c) Hematoxylin & Eosin staining of same tissue post-treatment demonstrates the damage observed in heat map (Stafford et al., 2011).

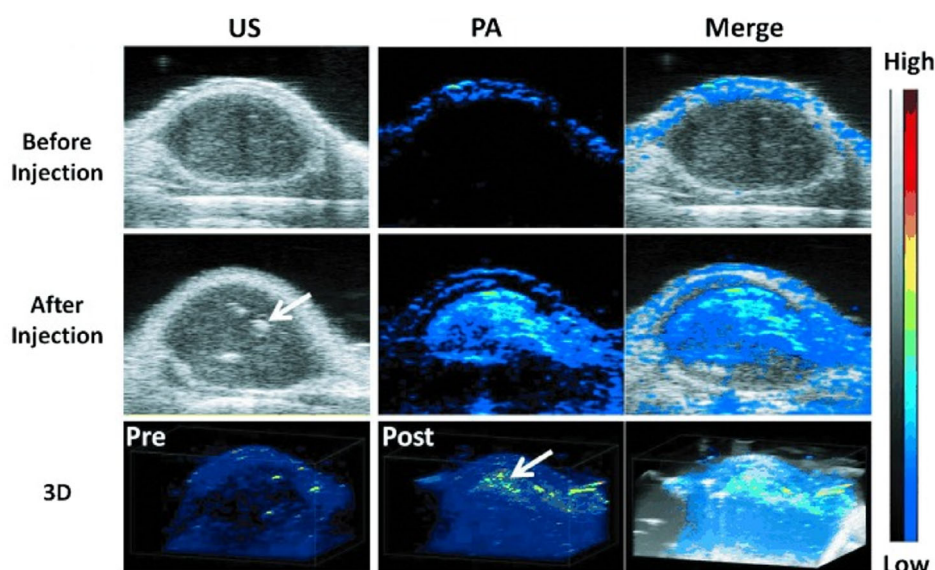


FIGURE 9 Ultrasound (US) and photoacoustic (PA) images with biodegradable gold nanovesicles postlaser light delivery. Combination of 2D ultrasonic (US) and photoacoustic (PA) in vivo images of MDA-MB-435 tumor-bearing mice exposed to 808 nm laser for 5 min postintravenous delivery of biodegradable gold nanovesicles. White arrows indicate nanoparticle signal (P. Huang et al., 2013).

several studies to linearly vary with tissue temperature changes within the range of 10–50°C, and algorithms have been developed to extract real-time temperature information by tracking temperature-induced changes in Γ parameter. For example, a novel interstitial PA sensor developed by Z. Li et al. (2015) used a single fiber coupler to deliver a combination of continuous-wave and pulsed laser light to ex vivo porcine liver tumor models. While the continuous-wave NIR light provided thermal irradiation leading to temperature elevation, the pulsed laser generated PA signal was utilized to extract temperature change information and assess tissue damage simultaneously. The PAI temperature measurements extracted with the bioheat equation were in good agreement with the control measurements made using thermocouples within the range of 22–55°C suggesting its potential in real-time temperature measurements and feedback control. In another recent study, Upputuri and coworkers (Upputuri et al., 2020) developed a pulsed laser diode (PLD)-based PATS system for temperature monitoring. The temperature information generated by PATS system in black ink and fresh animal blood was not only comparable to the data provided by the commercial fiber Bragg grating sensor but also provided temporal resolution of 1 ms and 0.31°C temperature sensitivity. Conclusively, although PAI-based thermometry enables real-time temperature profiling, the technique loses its accuracy beyond 50°C due to changes in tissue structure and morphology, such as protein denaturation and coagulation. This limits the use of PAI as a thermometry technique for nanoparticle-assisted LITT and requires further optimization.

4.3 | CT and PET

CT is another clinically used imaging procedure that has been shown to improve the diagnostic and therapeutic potential in clinical oncology due to its ability to provide 3D anatomical details of deep tissue with high resolution. Considering the high efficiency, low cost, easier accessibility, and convenience of imaging, it offers excellent potential for image-guided LITT treatment. Jermakowicz et al. (2016) evaluated using a mobile CT scanner, specifically Medtronic O-arm, for intraoperative frameless stereotaxic registration to confirm the navigation and laser catheter position during LITT procedure in patients with brain tumors. In comparison to standard preoperative CT scans, the use of O-arm allowed them to reduce the surgery time and patient discomfort without any complications. In addition, several efforts are being made to develop novel nanotheranostic platforms that can act as an efficient CT contrast agent for potential application in image-guided PTT treatment. For instance, J. Qin et al. (2015) demonstrated that gold nanorods injected into apolipoprotein E knockout mice not only produced high photothermal effect for treatment of macrophages in femoral artery restenosis but also exhibited excellent potential for use as CT contrast agent.

Nuclear imaging techniques such as PET that can reveal physiological changes by detecting chemical activity within cells have also been explored to evaluate the treatment effect of nanoparticle-based PTT either separately in combination with CT. Although PET imaging has primarily been used to track and localize radiolabelled copper nanoparticles (Cui et al., 2018), it can potentially be used as a tool for early evaluation of photothermal treatment response using the PET tracer ^{18}F -FDG, a radioisotope labeled glucose. In a recent study, Jørgensen et al. (2016) utilized ^{18}F -FDG PET imaging to compare the photothermal treatment response in tumor xenograft-bearing mice that were injected intratumorally with silica core gold nanoshells (vs. the control group) (Figure 10a) (Jørgensen et al., 2016). The thermographic imaging showed temperature elevation to 52 and 40°C in tumors treated with gold nanoshells and saline, respectively (Figure 10b) (Jørgensen et al., 2016). Importantly, PET imaging allowed them to evaluate the thermal response an hour after irradiation by quantifying the tumoral uptake of ^{18}F -FDG. They found that ^{18}F -FDG uptake was two-fold lower in mice treated with gold nanoshells in comparison to the saline group. Therefore, a combination of PET/CT dual imaging-guided PTT can potentially quantitate the efficiency of nanoparticle-assisted thermal treatment and detect morphological changes posttreatment. However, these studies have only been applied in preclinical settings and need further optimization before clinical applications.

4.4 | Fluorescence imaging and others

Fluorescence imaging is a widely used method for bioimaging cells and tissues in vitro and in vivo, and also has promising applications for fluorescence-guided surgery (Crawford et al., 2021; X. Li et al., 2021; Tanioka et al., 2021; Wolfbeis, 2015). Synthetic fluorescence probes and labels are used to make the sample of interest fluorescent. Alternatively, nanoparticles are an excellent fluorescent agent for improving brightness due to their unique characteristics of being inert within the microenvironment (Pratiwi et al., 2019; Wolfbeis, 2015). Emerging work has studied fluorescence

imaging using nanoparticles combined with interstitially delivered fiber optic cable or laser irradiation. The combination of fluorescence imaging using nanoparticles enables theranostic capabilities for tumor targeting and photothermal treatment (Zhao et al., 2017). For example, porphyrins are well known for their fluorescence and singlet oxygen

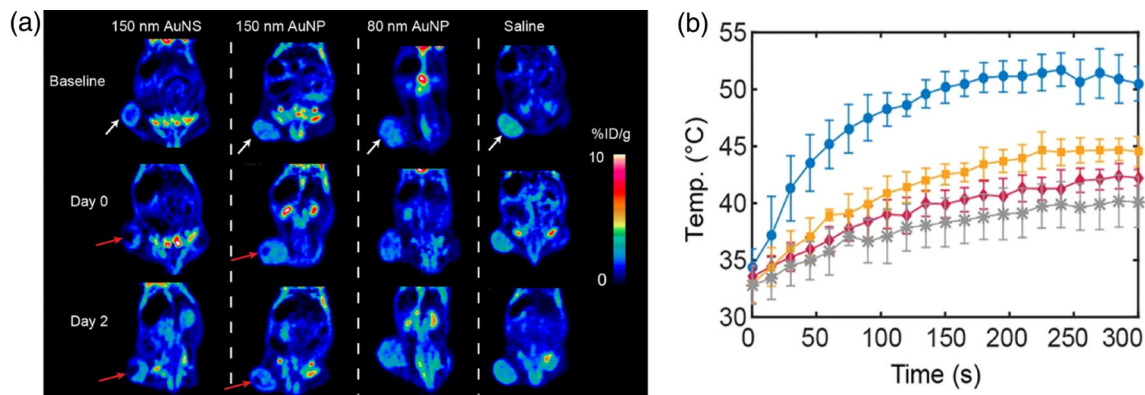


FIGURE 10 Positron emission tomography (PET) scan images and temperature profile of intratumorally delivered gold nanoparticles (AuNP). (a) PET scan images of mice treated with varying sizes of intratumorally delivered gold nanoparticles before laser irradiation (baseline), immediately after laser irradiation (Day 0), and 2 days after laser irradiation (Day 2). White arrows indicate delivery site of nanoparticles, while red arrows indicate decreased uptake of ^{18}F -FDG. Combination of PET/computed tomography (CT) image-guided PTT demonstrates potential to quantitate nanoparticle uptake efficiency for assisted thermal treatment in addition to detecting morphological changes posttreatment. (b) Plot of the temperature profiles based on time lapsed thermal images taken at the skin surface for each group (blue = gold nanoshells, yellow = 150-nm gold nanoparticles, red = 80-nm gold nanoparticles, gray = saline control) (Jørgensen et al., 2016).

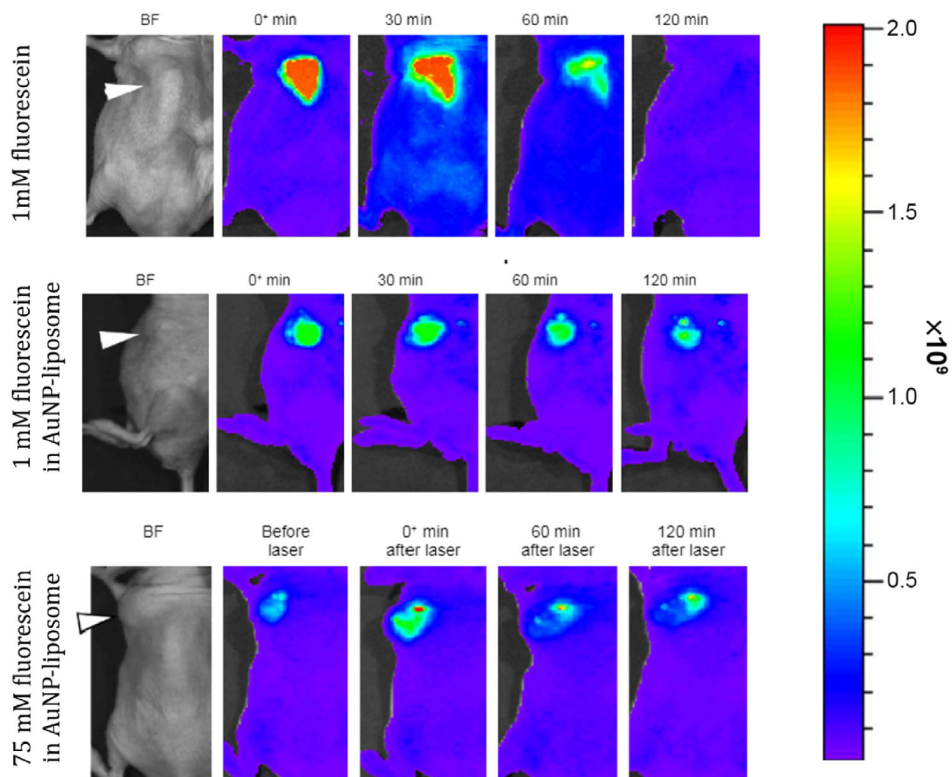


FIGURE 11 Fluorescence images postlaser activation and post-delivery of gold nanoparticle-liposomes loaded with fluorescein. Fluorescence images of fluorescein diffusion profiles demonstrating three different conditions (1 mM free fluorescein, 1 mM fluorescein loaded to gold nanoparticle-liposomes, and 75 mM fluorescein loaded to gold nanoparticle-liposomes) to demonstrate controlled and longer lasting delivery of fluorescein in a human breast cancer cell (MDA-MB 231 cells) xenograft mouse model (H. L. Huang et al., 2015)

generation upon laser light irradiation (Huynh & Zheng, 2014). Due to the highly dense porphyrin payload within the porphyrin, even a small amount of dissociated porphyrins resulted in strong fluorescence signals particularly advantageous for fluorescence imaging. Another study compared the delivery of free fluorescein to fluorescein delivered using a thermosensitive liposome embedded with gold nanoparticles. There was 5.79 times higher fluorescein retention within the tumor region when it was delivered using liposomes than administration without liposomes (Figure 11) (H. L. Huang et al., 2015).

Several other techniques, including infrared detectors (Morales-Cervantes et al., 2018), thermocouple probes (Manns et al., 1998), and thermal cameras (Y. Li et al., 2019), have been explored over the years to measure temperature changes during interstitial laser thermal treatment. Fiber optic sensors provide a promising approach for accurate real-time thermometry measurements in vivo with high spatial resolution and low cost. However, this technique is majorly limited because it can only provide one spatial temperature point rather than temperature distribution within the entire tissue (Schena et al., 2016; West et al., 2019). In addition, these sensors lose temperature accuracy as the distance increases from the fiber. To overcome these limitations, Ashikbayeva et al. (2020) recently implemented distributed sensing, specifically the optical backscattered reflectometry (OBR) technique, to monitor temperature changes in gold and magnetic iron oxide nanoparticle-assisted laser ablation in porcine liver phantoms. They employed four high scattering manganese oxide nanoparticle-doped fibers as optical sensors to record distributed temperature measurements over an area of 5.4 cm² by analyzing the back scattering profiles of nanoparticle-doped fibers to generate a two-dimensional (2D) map. The 2D thermal maps were generated with a resolution of 0.25 and 0.5 cm along the *x*-axis and *y*-axis, respectively.

Furthermore, the presence of gold and iron oxide nanoparticles during laser ablation led to temperature elevation from 88°C (in the absence of nanoparticles) to 162 and 111°C, respectively. In addition, laser treatment of tissue in the presence of gold nanoparticles demonstrated ablation of twice the area compared to tissue without nanoparticles. Although promising, this approach can lead to different outcomes depending on the tissue's fat content, optical properties, and sensitivity to strain and movements, emphasizing the need for further investigation.

5 | CONCLUSIONS

The two currently available FDA-approved LITT systems are exemplary products of advancements in image-guided technologies for treating unresectable tumors to help prolong overall patient survival. However, they been reported to have limitations in the context of brain tumors (Kim et al., 2020; Sharma et al., 2016; Sloan et al., 2013). Translation into the clinic should be a major focus when developing new technologies to combat these limitations during and especially before LITT treatments. Thus, the developing field of nanoparticle-assisted LITT is a very promising approach that allows for the seamless implementation of nanoparticles into the current LITT planning procedure as proposed in Figure 1. For the past several decades, nanoparticles have been utilized in various ways to better deliver treatments to patients. This includes utilization of nanoparticles as nanocarriers for drug delivery, dual-combination organic-inorganic nanoparticle formulations, and contrast agents to improve imaging and sensing (Bouché et al., 2021). Furthermore, the unique optical properties of particular nanoparticles (e.g., gold nanoparticles and porphyrin nanovesicles) enable efficient heat generation and heat localization within the tumor region. Other nanoparticle properties including customizable size, shape, and surface moieties also enable for selective cancer cell targeting (Y. Liu et al., 2015; Wu et al., 2010). Based on these properties, various types of models have been utilized to study and understand nanoparticles' role and impact on laser-tissue interactions for safer tumor ablation, specifically in relation to interstitial fiber optic delivery. For example, Nanospectra's™ Auroshell nanoparticle-assisted interstitial laser therapy is currently the first and only selectively targeted technology undergoing clinical trials to treat hard to reach prostate tumors. J.A. Schwartz et al. have extensively studied this approach in silico, in vitro, and in vivo canine models demonstrating successful selective temperature increase in the tumor tissue ($65.8 \pm 4.1^\circ\text{C}$) compared to sublethal temperature increase containing no nanoparticles in normal white and gray matter tissues ($48.6 \pm 1.1^\circ\text{C}$) (Schwartz et al., 2009).

There are also significant opportunities in the overall nanotechnology field to further develop certain components of the proposed workflow. This includes innovative strategies to deliver light instead of the currently used fiber optic cables. For example, Bagley et al. demonstrated direct implantation of a flexible NIR device to overcome light penetration depths to deliver interstitial photothermal therapy (Bagley et al., 2013). Lee et al. recently reported a synergistic hyaluronic-acid-based bioresorbable microneedle device for localized delivery of nanoparticles and high-energy photons to deliver photodynamic therapy and chemotherapy (Lee et al., 2021). Another example is the dual combination

inorganic/organic nanoparticle approach for controlled drug release within the tumor environment as demonstrated by H. L. Huang et al. and others (Al Zaki et al., 2014; H. L. Huang et al., 2015; McQuade et al., 2015).

Further future developments in this field are critical and may significantly impact the current MRI-guided LITT treatment and create exciting opportunities that can lead to a truly selective LITT system. To achieve successful outcomes, current obstacles for clinical translation and commercialization of both organic and inorganic nanoparticles need to be recognized and overcome (Anselmo & Mitragotri, 2015). For example, these formulations are far more complex compared to conventional drug delivery systems such as tablets and free-drug injections which have well-established large-scale manufacturing workflows (Hua et al., 2018). Therefore, current regulatory standards and manufacturing technologies need to be further adapted to better understand biocompatibility and safety in the perspective of material purity and quality (Marques et al., 2019; Sainz et al., 2015). In addition, addressing issues in current upstream and downstream manufacturing limitations to achieve a cost-effective and reproducible product can reduce risk in delaying clinical trial timelines (Marques et al., 2019).

AUTHOR CONTRIBUTIONS

Sumiao Pang: Conceptualization (equal); writing – original draft (lead); writing – review and editing (lead). **Anshika Kapur:** Writing – original draft (equal); writing – review and editing (equal). **Keri Zhou:** Writing – original draft (equal); writing – review and editing (equal). **Pavlos Anastasiadis:** Writing – original draft (supporting); writing – review and editing (equal). **Nicholas Ballirano:** Writing – original draft (supporting); writing – review and editing (equal). **Anthony J. Kim:** Conceptualization (equal); writing – review and editing (equal). **Jeffrey A. Winkles:** Conceptualization (equal); writing – review and editing (equal). **Graeme F. Woodworth:** Conceptualization (equal); writing – review and editing (equal). **Huang-Chiao Huang:** Conceptualization (lead); funding acquisition (lead); writing – original draft (equal); writing – review and editing (equal).

FUNDING INFORMATION

This work was supported by the University of Maryland start-up fund (Huang-Chiao Huang), Neuro-Link Award (Huang-Chiao Huang, Graeme F. Woodworth, Anthony J. Kim, Jeffrey A. Winkles), and National Institutes of Health (NIH) grants R01NS107813 (Graeme F. Woodworth) and R21EB028508 (Huang-Chiao Huang).

CONFLICT OF INTEREST

The authors have declared no conflicts of interest for this article.

DATA AVAILABILITY STATEMENT

Data sharing is not applicable to this article as no new data were created or analyzed in this study.

ORCID

Huang-Chiao Huang  <https://orcid.org/0000-0002-5406-0733>

RELATED WIREs ARTICLE

[Image-guided tumor surgery: The emerging role of nanotechnology](#)

REFERENCES

- Al Zaki, A., Joh, D., Cheng, Z., De Barros, A. L., Kao, G., Dorsey, J., & Tsourkas, A. (2014). Gold-loaded polymeric micelles for computed tomography-guided radiation therapy treatment and radiosensitization. *American Chemical Society Nano*, 8(1), 104–112. <https://doi.org/10.1021/nn405701q>
- Ali, M. R., Rahman, M. A., Wu, Y., Han, T., Peng, X., Mackey, M. A., Wang, D., Shin, H. J., Chen, Z. G., Xiao, H., Wu, R., Tang, Y., Shin, D. M., & el-Sayed, M. A. (2017). Efficacy, long-term toxicity, and mechanistic studies of gold nanorods photothermal therapy of cancer in xenograft mice. *Proceedings of the National Academy of Sciences of the United States of America*, 114(15), E3110–E3118. <https://doi.org/10.1073/pnas.1619302114>
- Anselmo, A. C., & Mitragotri, S. (2015). A review of clinical translation of inorganic nanoparticles. *The AAPS Journal*, 17(5), 1041–1054. <https://doi.org/10.1208/s12248-015-9780-2>
- Ashikbayeva, Z., Aitkulov, A., Jelbuldina, M., Issatayeva, A., Beisenova, A., Molardi, C., Saccomandi, P., Blanc, W., Inglezakis, V. J., & Tosi, D. (2020). Distributed 2D temperature sensing during nanoparticles assisted laser ablation by means of high-scattering fiber sensors. *Scientific Reports*, 10(1), 12593. <https://doi.org/10.1038/s41598-020-69384-2>

- Assi, H., Yang, C., Shaswary, E., Tam, M., Tavakkoli, J., Kolios, M., Peyman, G., & Kumaradas, C. (2021). Real-time control of nanoparticle-mediated thermal therapy using photoacoustic imaging. *IEEE Transactions on Biomedical Engineering*, 68(7), 2188–2194. <https://doi.org/10.1109/TBME.2020.3037991>
- Bagley, A. F., Hill, S., Rogers, G. S., & Bhatia, S. N. (2013). Plasmonic photothermal heating of intraperitoneal tumors through the use of an implanted near-infrared source. *American Chemical Society Nano*, 7(9), 8089–8097. <https://doi.org/10.1021/nn4033757>
- Barenholz, Y. (2012). Doxil[®]—The first FDA-approved nano-drug: Lessons learned. *Journal of Controlled Release*, 160(2), 117–134. <https://doi.org/10.1016/j.jconrel.2012.03.020>
- Bayazitoglu, Y., Kheradmand, S. h., & Tullius, T. K. (2013). An overview of nanoparticle assisted laser therapy. *International Journal of Heat and Mass Transfer*, 67, 469–486. <https://doi.org/10.1016/j.ijheatmasstransfer.2013.08.018>
- Biggins, J. S., Yazdi, S., & Ringe, E. (2018). Magnesium nanoparticle plasmonics. *Nano Letters*, 18(6), 3752–3758. <https://doi.org/10.1021/acs.nanolett.8b00955>
- Bouché, M., Dong, Y. C., Sheikh, S., Taing, K., Saxena, D., Hsu, J. C., Chen, M. H., Salinas, R. D., Song, H., Burdick, J. A., Dorsey, J., & Cormode, D. P. (2021). Novel treatment for glioblastoma delivered by a radiation responsive and radiopaque hydrogel. *American Chemical Society Biomaterials Science & Engineering*, 7(7), 3209–3220. <https://doi.org/10.1021/acsbiomaterials.1c00385>
- Chongsathidkiet, P., Liu, Y., Kemeny, H., Dechant, C., Odion, R., Cui, X., Rhodin, K., Vo-Dinh, T., & Fecci, P. (2018). EXTH-23. A novel nanotechnology-based platform improves laser interstitial thermal therapy for intracranial tumors. *Neuro-Oncology*, 20, vi89. <https://doi.org/10.1093/neuonc/noy148.372>
- Chu, Z., Wang, Z., Chen, L., Wang, X., Huang, C., Cui, M., Yang, D. P., & Jia, N. (2018). Combining magnetic resonance imaging with photothermal therapy of CuS@BSA nanoparticles for cancer theranostics. *American Chemical Society Applied Nano Materials*, 1(5), 2332–2340. <https://doi.org/10.1021/acsanm.8b00410>
- Crawford, K. L., Pacheco, F. V., Lee, Y. J., Hom, M., Rosenthal, E. L., Nguyen, Q. T., & Orosco, R. K. (2021). A scoping review of ongoing fluorescence-guided surgery clinical trials in otolaryngology. *The Laryngoscope*, 132, 36–44. <https://doi.org/10.1002/lary.29891>
- Cui, L., Xiong, C., Zhou, M., Shi, S., Chow, D. S. L., & Li, C. (2018). Integrin $\alpha\beta 3$ -targeted [64Cu]CuS nanoparticles for PET/CT imaging and photothermal ablation therapy. *Bioconjugate Chemistry*, 29(12), 4062–4071. <https://doi.org/10.1021/acs.bioconjchem.8b00690>
- De Poorter, J. (1995). Noninvasive MRI thermometry with the proton resonance frequency method: Study of susceptibility effects. *Magnetic Resonance in Medicine*, 34(3), 359–367. <https://doi.org/10.1002/mrm.1910340313>
- Dickerson, E. B., Dreaden, E. C., Huang, X., el-Sayed, I. H., Chu, H., Pushpanketh, S., McDonald, J., & el-Sayed, M. A. (2008). Gold nanorod assisted near-infrared plasmonic photothermal therapy (PPTT) of squamous cell carcinoma in mice. *Cancer Letters*, 269(1), 57–66. <https://doi.org/10.1016/j.canlet.2008.04.026>
- Dou, Y. N., Zheng, J., Foltz, W. D., Weersink, R., Chaudary, N., Jaffray, D. A., & Allen, C. (2014). Heat-activated thermosensitive liposomal cisplatin (HTLC) results in effective growth delay of cervical carcinoma in mice. *Journal of Controlled Release*, 178, 69–78. <https://doi.org/10.1016/j.jconrel.2014.01.009>
- D'Souza, W. D., Madsen, E. L., Unal, O., Vigen, K. K., Frank, G. R., & Thomadsen, B. R. (2001). Tissue mimicking materials for a multi-imaging modality prostate phantom. *Medical Physics*, 28(4), 688–700. <https://doi.org/10.1118/1.1354998>
- Elliott, A. M., Schwartz, J., Wang, J., Shetty, A. M., Bourgoyne, C., O'Neal, D. P., Hazle, J. D., & Stafford, R. J. (2009). Quantitative comparison of delta P1 versus optical diffusion approximations for modeling near-infrared gold nanoshell heating. *Medical Physics*, 36(4), 1351–1358. <https://doi.org/10.1118/1.3056456>
- Elliott, A. M., Shetty, A. M., Wang, J., Hazle, J. D., & Jason Stafford, R. (2010). Use of gold nanoshells to constrain and enhance laser thermal therapy of metastatic liver tumours. *International Journal of Hyperthermia*, 26(5), 434–440. <https://doi.org/10.3109/02656731003685805>
- El-Sayed, I. H., Huang, X., & El-Sayed, M. A. (2006). Selective laser photo-thermal therapy of epithelial carcinoma using anti-EGFR antibody conjugated gold nanoparticles. *Cancer Letters*, 239(1), 129–135. <https://doi.org/10.1016/j.canlet.2005.07.035>
- Fuentes, D., Elliott, A., Weinberg, J. S., Shetty, A., Hazle, J. D., & Stafford, R. J. (2013). An inverse problem approach to recovery of in vivo nanoparticle concentrations from thermal image monitoring of MR-guided laser induced thermal therapy. *Annals of Biomedical Engineering*, 41(1), 100–111. <https://doi.org/10.1007/s10439-012-0638-9>
- Gad, S. C., Sharp, K. L., Montgomery, C., Payne, J. D., & Goodrich, G. P. (2012). Evaluation of the toxicity of intravenous delivery of auroshell particles (gold-silica nanoshells). *International Journal of Toxicology*, 31(6), 584–594. <https://doi.org/10.1177/1091581812465969>
- Gebhart, S. C., Lin, W. C., & Mahadevan-Jansen, A. (2006). In vitro determination of normal and neoplastic human brain tissue optical properties using inverse adding-doubling. *Physics in Medicine and Biology*, 51(8), 2011–2027. <https://doi.org/10.1088/0031-9155/51/8/004>
- Germer, C. T., Roggan, A., Ritz, J. P., Isbert, C., Albrecht, D., Müller, G., & Buhr, H. J. (1998). Optical properties of native and coagulated human liver tissue and liver metastases in the near infrared range. *Lasers in Surgery and Medicine*, 23(4), 194–203. [https://doi.org/10.1002/\(sici\)1096-9101\(1998\)23:4<194::aid-lsm2>3.0.co;2-6](https://doi.org/10.1002/(sici)1096-9101(1998)23:4<194::aid-lsm2>3.0.co;2-6)
- Grauer, O., Jaber, M., Hess, K., Weckesser, M., Schwindt, W., Maring, S., Wölfer, J., & Stummer, W. (2019). Combined intracavitary thermotherapy with iron oxide nanoparticles and radiotherapy as local treatment modality in recurrent glioblastoma patients. *Journal of Neuro-Oncology*, 141(1), 83–94. <https://doi.org/10.1007/s11060-018-03005-x>
- Haj-Hosseini, N., Kistler, B., & Wärdell, K. (2014). Development and characterization of a brain tumor mimicking fluorescence phantom. *Society of Photo-optical Instrumentation Engineers*, 8945(894505), 1–6. <https://doi.org/10.1117/12.2039861>
- Hastman, D. A., Melinger, J. S., Aragonés, G. L., Cunningham, P. D., Chiriboga, M., Salvato, Z. J., Salvato, T. M., Brown, C. W., 3rd, Mathur, D., Medintz, I. L., Oh, E., & Díaz, S. A. (2020). Femtosecond laser pulse excitation of DNA-labeled gold nanoparticles:

- Establishing a quantitative local nanothermometer for biological applications. *American Chemical Society Nano*, 14(7), 8570–8583. <https://doi.org/10.1021/acs.nano.0c02899>
- Higbee-Dempsey, E. M., Amirshaghghi, A., Case, M. J., Bouché, M., Kim, J., Cormode, D. P., & Tsourkas, A. (2020). Biodegradable gold nanoclusters with improved excretion due to pH-triggered hydrophobic-to-hydrophilic transition. *Journal of the American Chemical Society*, 142(17), 7783–7794. <https://doi.org/10.1021/jacs.9b13813>
- Hua, S., de Matos, M. B. C., Metselaar, J. M., & Storm, G. (2018). Current trends and challenges in the clinical translation of nanoparticulate nanomedicines: Pathways for translational development and commercialization. *Frontiers in Pharmacology*, 9, 790. <https://doi.org/10.3389/fphar.2018.00790>
- Huang, H. C., Barua, S., Kay, D. B., & Rege, K. (2009). Simultaneous enhancement of photothermal stability and gene delivery efficacy of gold nanorods using polyelectrolytes. *American Chemical Society Nano*, 3(10), 2941–2952. <https://doi.org/10.1021/nn900947a>
- Huang, H. C., Rege, K., & Heys, J. J. (2010). Spatiotemporal temperature distribution and cancer cell death in response to extracellular hyperthermia induced by gold nanorods. *American Chemical Society Nano*, 4(5), 2892–2900. <https://doi.org/10.1021/nn901884d>
- Huang, H. L., Lu, P. H., Yang, H. C., Lee, G. D., Li, H. R., & Liao, K. C. (2015). Fiber-optic triggered release of liposome in vivo: Implication of personalized chemotherapy. *International Journal of Nanomedicine*, 10, 5171–5184. <https://doi.org/10.2147/ijn.s85915>
- Huang, P., Lin, J., Li, W., Rong, P., Wang, Z., Wang, S., Wang, X., Sun, X., Aronova, M., Niu, G., Leapman, R. D., Nie, Z., & Chen, X. (2013). Biodegradable gold nanovesicles with an ultrastrong plasmonic coupling effect for photoacoustic imaging and photothermal therapy. *Angewandte Chemie International Edition*, 52(52), 13958–13964. <https://doi.org/10.1002/anie.201308986>
- Huang, X., El-Sayed, I. H., Qian, W., & El-Sayed, M. A. (2006). Cancer cell imaging and photothermal therapy in the near-infrared region by using gold nanorods. *Journal of the American Chemical Society*, 128(6), 2115–2120. <https://doi.org/10.1021/ja057254a>
- Huang, X., Jain, P. K., El-Sayed, I. H., & El-Sayed, M. A. (2006). Determination of the minimum temperature required for selective photothermal destruction of cancer cells with the use of immunotargeted gold nanoparticles. *Photochemistry and Photobiology*, 82(2), 412–417. <https://doi.org/10.1562/2005-12-14-RA-754>
- Huang, X., Jain, P. K., El-Sayed, I. H., & El-Sayed, M. A. (2007). Gold nanoparticles: Interesting optical properties and recent applications in cancer diagnostics and therapy. *Nanomedicine (London, England)*, 2(5), 681–693. <https://doi.org/10.2217/17435889.2.5.681>
- Huynh, E., & Zheng, G. (2014). Porphyosome nanotechnology: A paradigm shift in lipid-based supramolecular structures. *NanoToday*, 9(2), 212–222. <https://doi.org/10.1016/j.nantod.2014.04.012>
- Jeon, K. J., Moon, H. R., Ruminski, A. M., Jiang, B., Kisielowski, C., Bardhan, R., & Urban, J. J. (2011). Air-stable magnesium nanocomposites provide rapid and high-capacity hydrogen storage without using heavy-metal catalysts. *Nature Materials*, 10(4), 286–290. <https://doi.org/10.1038/nmat2978>
- Jermakowicz, W. J., Diaz, R. J., Cass, S. H., Ivan, M. E., & Komotar, R. J. (2016). Use of a mobile intraoperative computed tomography scanner for navigation registration during laser interstitial thermal therapy of brain tumors. *World Neurosurgery*, 94, 418–425. <https://doi.org/10.1016/j.wneu.2016.06.126>
- Jin, C. S., Wada, H., Anayama, T., McVeigh, P. Z., Hu, H. P., Hirohashi, K., Nakajima, T., Kato, T., Keshavjee, S., Hwang, D., Wilson, B. C., Zheng, G., & Yasufuku, K. (2016). An integrated nanotechnology-enabled transbronchial image-guided intervention strategy for peripheral lung cancer. *Cancer Research*, 76(19), 5870–5880. <https://doi.org/10.1158/0008-5472.CAN-15-3196>
- Jørgensen, J. T., Norregaard, K., Tian, P., Bendix, P. M., Kjaer, A., & Oddershede, L. B. (2016). Single particle and PET-based platform for identifying optimal plasmonic nano-heaters for photothermal cancer therapy. *Scientific Reports*, 6, 30076. <https://doi.org/10.1038/srep30076>
- Kamath, A. A., Friedman, D. D., Hacker, C. D., Smyth, M. D., Limbrick, D. D., Kim, A. H., Hawasli, A. H., & Leuthardt, E. C. (2017). MRI-guided interstitial laser ablation for intracranial lesions: A large single-institution experience of 133 cases. *Stereotactic and Functional Neurosurgery*, 95(6), 417–428. <https://doi.org/10.1159/000485387>
- Kannadorai, R. K., & Liu, Q. (2013). Optimization in interstitial plasmonic photothermal therapy for treatment planning. *Medical Physics*, 40(10), 103301. <https://doi.org/10.1118/1.4810935>
- Kim, A. H., Tatter, S., Rao, G., Prabhu, S., Chen, C., Fecci, P., Chiang, V., Smith, K., Williams, B. J., Mohammadi, A. M., Judy, K., Sloan, A., Tovar-Spinoza, Z., Baumgartner, J., Hadjipanayis, C., & Leuthardt, E. C. (2020). Laser ablation of abnormal neurological tissue using robotic neuroplate system (LAANTERN): 12-month outcomes and quality of life after brain tumor ablation. *Neurosurgery*, 87(3), E338–E346. <https://doi.org/10.1093/neuros/nyaa071>
- Knights, O., Freear, S., & McLaughlan, J. R. (2020). Improving plasmonic photothermal therapy of lung cancer cells with anti-EGFR targeted gold nanorods. *Nanomaterials (Basel, Switzerland)*, 10(7), 1307. <https://doi.org/10.3390/nano10071307>
- Lancet, J. E., Uy, G. L., Newell, L. F., Lin, T. L., Ritchie, E. K., Stuart, R. K., Strickland, S. A., Hogge, D., Solomon, S. R., Bixby, D. L., Kolitz, J. E., Schiller, G. J., Wieduwilt, M. J., Ryan, D. H., Faderl, S., & Cortes, J. E. (2021). CPX-351 versus 7+3 cytarabine and daunorubicin chemotherapy in older adults with newly diagnosed high-risk or secondary acute myeloid leukaemia: 5-year results of a randomised, open-label, multicentre, phase 3 trial. *The Lancet Haematology*, 8(7), e481–e491. [https://doi.org/10.1016/S2352-3026\(21\)00134-4](https://doi.org/10.1016/S2352-3026(21)00134-4)
- Lee, Y., Kang, T., Cho, H. R., Lee, G. J., Park, O. K., Kim, S., Lee, B., Kim, H. M., Cha, G. D., Shin, Y., Lee, W., Kim, M., Kim, H., Song, Y. M., Choi, S. H., Hyeon, T., & Kim, D. H. (2021). Localized delivery of theranostic nanoparticles and high-energy photons using microneedles-on-bioelectronics. *Advanced Materials*, 33(24), e2100425. <https://doi.org/10.1002/adma.202100425>
- Leung, J. P., Wu, S., Chou, K. C., & Signorell, R. (2013). Investigation of Sub-100 nm gold nanoparticles for laser-induced thermotherapy of cancer. *Nanomaterials (Basel)*, 3(1), 86–106. <https://doi.org/10.3390/nano3010086>

- Li, X., Wu, P., Cao, W., & Xiong, H. (2021). Development of pH-activatable fluorescent probes for rapid visualization of metastatic tumours and fluorescence-guided surgery. *Chemical Communication*, 57(81), 10636–10639. <https://doi.org/10.1039/d1cc04408g>
- Li, Y., Li, X., Doughty, A., West, C., Wang, L., Zhou, F., Nordquist, R. E., & Chen, W. R. (2019). Phototherapy using immunologically modified carbon nanotubes to potentiate checkpoint blockade for metastatic breast cancer. *Nanomedicine*, 18, 44–53. <https://doi.org/10.1016/j.nano.2019.02.009>
- Li, Z., Chen, H., Zhou, F., Li, H., & Chen, W. R. (2015). Interstitial photoacoustic sensor for the measurement of tissue temperature during interstitial laser phototherapy. *Sensors (Basel, Switzerland)*, 15(3), 5583–5593. <https://doi.org/10.3390/s150305583>
- Liu, S., Doughty, A., West, C., Tang, Z., Zhou, F., & Chen, W. R. (2018). Determination of temperature distribution in tissue for interstitial cancer photothermal therapy. *International Journal of Hyperthermia*, 34(6), 756–763. <https://doi.org/10.1080/02656736.2017.1370136>
- Liu, T., Zhang, M., Liu, W., Zeng, X., Song, X., Yang, X., Zhang, X., & Feng, J. (2018). Metal ion/tannic acid assembly as a versatile photothermal platform in engineering multimodal nanotheranostics for advanced applications. *American Chemical Society Nano*, 12(4), 3917–3927. <https://doi.org/10.1021/acsnano.8b01456>
- Liu, Y., Ashton, J. R., Moding, E. J., Yuan, H., Register, J. K., Fales, A. M., Choi, J., Whitley, M. J., Zhao, X., Qi, Y., Ma, Y., Vaidyanathan, G., Zalutsky, M. R., Kirsch, D. G., Badea, C. T., & Vo-Dinh, T. (2015). A plasmonic gold nanostar theranostic probe for in vivo tumor imaging and photothermal therapy. *Theranostics*, 5(9), 946–960. <https://doi.org/10.7150/thno.11974>
- Liu, Y., Bhattarai, P., Dai, Z., & Chen, X. (2019). Photothermal therapy and photoacoustic imaging via nanotheranostics in fighting cancer. *Chemical Society Reviews*, 48(7), 2053–2108. <https://doi.org/10.1039/C8CS00618K>
- Liu, Y., Yang, X., Huang, Z., Huang, P., Zhang, Y., Deng, L., Wang, Z., Zhou, Z., Liu, Y., Kalish, H., Khachab, N. M., Chen, X., & Nie, Z. (2016). Magneto-plasmonic Janus vesicles for magnetic field-enhanced photoacoustic and magnetic resonance imaging of tumors. *Angewandte Chemie (International Ed. in English)*, 55(49), 15297–15300. <https://doi.org/10.1002/anie.201608338>
- Loo, C., Lin, A., Hirsch, L., Lee, M. H., Barton, J., Halas, N., West, J., & Drezek, R. (2004). Nanoshell-enabled photonics-based imaging and therapy of cancer. *Technology in Cancer Research & Treatment*, 3(1), 33–40. <https://doi.org/10.1177/153303460400300104>
- Loo, C., Lowery, A., Halas, N., West, J., & Drezek, R. (2005). Immunotargeted nanoshells for integrated cancer imaging and therapy. *Nano Letters*, 5(4), 709–711. <https://doi.org/10.1021/nl050127s>
- Lovell, J. F., Jin, C. S., Huynh, E., Jin, H., Kim, C., Rubinstein, J. L., Chan, W. C., Cao, W., Wang, L. V., & Zheng, G. (2011). Porphysome nanovesicles generated by porphyrin bilayers for use as multimodal biophotonic contrast agents. *Nature Materials*, 10(4), 324–332. <https://doi.org/10.1038/nmat2986>
- Ma, M., Chen, H., Chen, Y., Wang, X., Chen, F., Cui, X., & Shi, J. (2012). Au capped magnetic core/mesoporous silica shell nanoparticles for combined photothermo-/chemo-therapy and multimodal imaging. *Biomaterials*, 33(3), 989–998. <https://doi.org/10.1016/j.biomaterials.2011.10.017>
- MacDonald, T. D., Liu, T. W., & Zheng, G. (2014). An MRI-sensitive, non-photobleachable porphysome photothermal agent. *Angewandte Chemie (International Ed. in English)*, 53(27), 6956–6959. <https://doi.org/10.1002/anie.201400133>
- Mahmoudi, K., Bouras, A., Bozec, D., Ivkov, R., & Hadjipanayis, C. (2018). Magnetic hyperthermia therapy for the treatment of glioblastoma: A review of the therapy's history, efficacy and application in humans. *International Journal of Hyperthermia*, 34, 1316–1328. <https://doi.org/10.1080/02656736.2018.1430867>
- Man, J., Shoemaker, J. D., Ma, T., Rizzo, A. E., Godley, A. R., Wu, Q., Mohammadi, A. M., Bao, S., Rich, J. N., & Yu, J. S. (2015). Hyperthermia sensitizes glioma stem-like cells to radiation by inhibiting AKT signaling. *Cancer Research*, 75(8), 1760–1769. <https://doi.org/10.1158/0008-5472.CAN-14-3621>
- Manns, F., Milne, P. J., Gonzalez-Cirre, X., Denham, D. B., Parel, J. M., & Robinson, D. S. (1998). In situ temperature measurements with thermocouple probes during laser interstitial thermotherapy (LITT): Quantification and correction of a measurement artifact. *Lasers in Surgery and Medicine*, 23(2), 94–103. [https://doi.org/10.1002/\(sici\)1096-9101\(1998\)23:2<94::aid-lsm7>3.0.co;2-q](https://doi.org/10.1002/(sici)1096-9101(1998)23:2<94::aid-lsm7>3.0.co;2-q)
- Marques, M. R. C., Choo, Q., Ashtikar, M., Rocha, T. C., Bremer-Hoffmann, S., & Wacker, M. G. (2019). Nanomedicines—Tiny particles and big challenges. *Advanced Drug Delivery Reviews*, 151–152, 23–43. <https://doi.org/10.1016/j.addr.2019.06.003>
- McQuade, C., Al Zaki, A., Desai, Y., Vido, M., Sakhuja, T., Cheng, Z., Hickey, R. J., Joh, D., Park, S. J., Kao, G., Dorsey, J. F., & Tsourkas, A. (2015). A multifunctional nanoplatform for imaging, radiotherapy, and the prediction of therapeutic response. *Small*, 11(7), 834–843. <https://doi.org/10.1002/sml.201401927>
- Medvid, R., Ruiz, A., Komotar, R. J., Jagid, J. R., Ivan, M. E., Quencer, R. M., & Desai, M. B. (2015). Current applications of MRI-guided laser interstitial thermal therapy in the treatment of brain neoplasms and epilepsy: A radiologic and neurosurgical overview. *AJNR. American Journal of Neuroradiology*, 36(11), 1998–2006. <https://doi.org/10.3174/ajnr.A4362>
- Meng, L., Deschaume, O., Larbanoix, L., Fron, E., Bartic, C., Laurent, S., Van der Auweraer, M., & Glorieux, C. (2019). Photoacoustic temperature imaging based on multi-wavelength excitation. *Photoacoustics*, 13, 33–45. <https://doi.org/10.1016/j.pacs.2018.11.004>
- Morales-Cervantes, A., Kolosovas-Machuca, E. S., Guevara, E., Maruris Reducindo, M., Bello Hernández, A. B., Ramos García, M., & González, F. J. (2018). An automated method for the evaluation of breast cancer using infrared thermography. *EXCLI Journal*, 17, 989–998. <https://doi.org/10.17179/excli2018-1735>
- Muhanna, N., Jin, C. S., Huynh, E., Chan, H., Qiu, Y., Jiang, W., Cui, L., Burgess, L., Akens, M. K., Chen, J., Irish, J. C., & Zheng, G. (2015). Phototheranostic porphyrin nanoparticles enable visualization and targeted treatment of head and neck cancer in clinically relevant models. *Theranostics*, 5(12), 1428–1443. <https://doi.org/10.7150/thno.13451>
- Nikoobakht, B., & El-Sayed, M. A. (2003). Preparation and growth mechanism of gold nanorods (NRs) using seed-mediated growth method. *Chemistry of Materials*, 15(10), 1957–1962. <https://doi.org/10.1021/cm020732l>
- Panchapakesan, B., Book-Newell, B., Sethu, P., Rao, M., & Irudayaraj, J. (2011). Gold nanoprobe for theranostics. *Nanomedicine (London, England)*, 6(10), 1787–1811. <https://doi.org/10.2217/nnm.11.155>

- Patel, P., Patel, N. V., & Danish, S. F. (2016). Intracranial MR-guided laser-induced thermal therapy: Single-center experience with the Visualase thermal therapy system. *Journal of Neurosurgery*, 125(4), 853–860. <https://doi.org/10.3171/2015.7.JNS15244>
- Patel, T. R., & Chiang, V. L. S. (2014). Laser interstitial thermal therapy for treatment of post-radiosurgery tumor recurrence and radiation necrosis. *Photonics & Lasers in Medicine*, 3(2), 95–105. <https://doi.org/10.1515/plm-2013-0057>
- Perez, J. G., Tran, N. L., Rosenblum, M. G., Schneider, C. S., Connolly, N. P., Kim, A. J., Woodworth, G. F., & Winkles, J. A. (2016). The TWEAK receptor Fn14 is a potential cell surface portal for targeted delivery of glioblastoma therapeutics. *Oncogene*, 35(17), 2145–2155. <https://doi.org/10.1038/onc.2015.310>
- Phan, T. T. V., Bui, N. Q., Cho, S.-W., Bharathiraja, S., Manivasagan, P., Moorthy, M. S., Mondal, S., Kim, C. S., & Oh, J. (2018). Photoacoustic imaging-guided photothermal therapy with tumor-targeting HA-FeOOH@PPy nanorods. *Scientific Reports*, 8(1), 8809. <https://doi.org/10.1038/s41598-018-27204-8>
- Pratiwi, F. W., Kuo, C. W., Chen, B. C., & Chen, P. (2019). Recent advances in the use of fluorescent nanoparticles for bioimaging. *Nanomedicine (London, England)*, 14(13), 1759–1769. <https://doi.org/10.2217/nnm-2019-0105>
- Qin, J., Peng, Z., Li, B., Ye, K., Zhang, Y., Yuan, F., Yang, X., Huang, L., Hu, J., & Lu, X. (2015). Gold nanorods as a theranostic platform for in vitro and in vivo imaging and photothermal therapy of inflammatory macrophages. *Nanoscale*, 7(33), 13991–14001. <https://doi.org/10.1039/C5NR02521D>
- Qin, Z., & Bischof, J. C. (2012). Thermophysical and biological responses of gold nanoparticle laser heating. *Chemical Society Reviews*, 41(3), 1191–1217. <https://doi.org/10.1039/c1cs15184c>
- Quesson, B., de Zwart, J. A., & Moonen, C. T. (2000). Magnetic resonance temperature imaging for guidance of thermotherapy. *Journal of Magnetic Resonance Imaging*, 12(4), 525–533. [https://doi.org/10.1002/1522-2586\(200010\)12:4<525::aid-jmri3>3.0.co;2-v](https://doi.org/10.1002/1522-2586(200010)12:4<525::aid-jmri3>3.0.co;2-v)
- Rastinehad, A. R., Anastos, H., Wajswol, E., Winoker, J. S., Sfakianos, J. P., Doppalapudi, S. K., Carrick, M. R., Knauer, C. J., Taouli, B., Lewis, S. C., Tewari, A. K., Schwartz, J. A., Canfield, S. E., George, A. K., West, J. L., & Halas, N. J. (2019). Gold nanoshell-localized photothermal ablation of prostate tumors in a clinical pilot device study. *Proceedings of the National Academy of Sciences of the United States of America*, 116(37), 18590–18596. <https://doi.org/10.1073/pnas.1906929116>
- Ren, Y., Qi, H., Chen, Q., & Ruan, L. (2017). Thermal dosage investigation for optimal temperature distribution in gold nanoparticle enhanced photothermal therapy. *International Journal of Heat and Mass Transfer*, 106, 212–221. <https://doi.org/10.1016/j.ijheatmasstransfer.2016.10.067>
- Revia, R. A., & Zhang, M. (2016). Magnetite nanoparticles for cancer diagnosis, treatment, and treatment monitoring: Recent advances. *Materials Today (Kidlington)*, 19(3), 157–168. <https://doi.org/10.1016/j.mattod.2015.08.022>
- Sainz, V., Connot, J., Matos, A. I., Peres, C., Zupancic, E., Moura, L., Silva, L. C., Florindo, H. F., & Gaspar, R. S. (2015). Regulatory aspects on nanomedicines. *Biochemical and Biophysical Research Communications*, 468(3), 504–510. <https://doi.org/10.1016/j.bbrc.2015.08.023>
- Salem, U., Kumar, V. A., Madewell, J. E., Schomer, D. F., de Almeida Bastos, D. C., Zinn, P. O., Weinberg, J. S., Rao, G., Prabhu, S. S., & Colen, R. R. (2019). Neurosurgical applications of MRI guided laser interstitial thermal therapy (LITT). *Cancer Imaging*, 19(1), 65. <https://doi.org/10.1186/s40644-019-0250-4>
- Schena, E., Tosi, D., Saccomandi, P., Lewis, E., & Kim, T. (2016). Fiber optic sensors for temperature monitoring during thermal treatments: An overview. *Sensors (Basel, Switzerland)*, 16(7), 1144. <https://doi.org/10.3390/s16071144>
- Schneider, C. S., Woodworth, G. F., Vujaskovic, Z., & Mishra, M. V. (2020). Radiosensitization of high-grade gliomas through induced hyperthermia: Review of clinical experience and the potential role of MR-guided focused ultrasound. *Radiotherapy and Oncology*, 142, 43–51. <https://doi.org/10.1016/j.radonc.2019.07.017>
- Schwartz, J. A., Price, R. E., Gill-Sharp, K. L., Sang, K. L., Khorchani, J., Goodwin, B. S., & Payne, J. D. (2011). Selective nanoparticle-directed ablation of the canine prostate. *Lasers in Surgery and Medicine*, 43(3), 213–220. <https://doi.org/10.1002/lsm.21039>
- Schwartz, J. A., Shetty, A. M., Price, R. E., Stafford, R. J., Wang, J. C., Uthamanthil, R. K., Pham, K., McNichols, R., Coleman, C. L., & Payne, J. D. (2009). Feasibility study of particle-assisted laser ablation of brain tumors in orthotopic canine model. *Cancer Research*, 69(4), 1659–1667. <https://doi.org/10.1158/0008-5472.CAN-08-2535>
- Schwarzmaier, H.-J., Eickmeyer, F., Fiedler, V. U., & Ulrich, F. (2002). Basic principles of laser induced interstitial thermotherapy in brain tumors. *Medical Laser Application*, 17, 147–158. [10.1078/1615-1615-00547](https://doi.org/10.1078/1615-1615-00547)
- Sharma, M., Habboub, G., Behbahani, M., Silva, D., Barnett, G. H., & Mohammadi, A. M. (2016). Thermal injury to corticospinal tracts and postoperative motor deficits after laser interstitial thermal therapy. *Neurosurgical Focus*, 41(4), E6. <https://doi.org/10.3171/2016.7.FOCUS16216>
- Sloan, A. E., Ahluwalia, M. S., Valerio-Pascua, J., Manjila, S., Torchia, M. G., Jones, S. E., Sunshine, J. L., Phillips, M., Griswold, M. A., Clampitt, M., Brewer, C., Jochum, J., McGraw, M. V., Diorio, D., Ditz, G., & Barnett, G. H. (2013). Results of the NeuroBlate system first-in-humans phase I clinical trial for recurrent glioblastoma: Clinical article. *Journal of Neurosurgery*, 118(6), 1202–1219. <https://doi.org/10.3171/2013.1.JNS1291>
- Stabile, J., Najafali, D., Cheema, Y., Inglut, C. T., Liang, B. J., Vaja, S., Sorrin, A. J., & Huang, H.-C. (2020). Chapter 12—Engineering gold nanoparticles for photothermal therapy, surgery, and imaging. In *Nanomaterials for biomedical applications*. Elsevier. <https://doi.org/10.1016/B978-0-12-816662-8.00012-6>
- Stafford, R. J., Shetty, A., Elliott, A. M., Schwartz, J. A., Goodrich, G. P., & Hazle, J. D. (2011). MR temperature imaging of nanoshell mediated laser ablation. *International Journal of Hyperthermia*, 27(8), 782–790. <https://doi.org/10.3109/02656736.2011.614671>
- Stern, J. M., Kibanov Solomonov, V. V., Sazykina, E., Schwartz, J. A., Gad, S. C., & Goodrich, G. P. (2016). Initial evaluation of the safety of nanoshell-directed photothermal therapy in the treatment of prostate disease. *International Journal of Toxicology*, 35(1), 38–46. <https://doi.org/10.1177/1091581815600170>

- Stewart, D. C., Rubiano, A., Dyson, K., & Simmons, C. S. (2017). Mechanical characterization of human brain tumors from patients and comparison to potential surgical phantoms. *PLoS One*, *12*(6), e0177561. <https://doi.org/10.1371/journal.pone.0177561>
- Tang, J., Gao, K., Ou, Q., Fu, X., Man, S. Q., Guo, J., & Liu, Y. (2018). Calculation extinction cross sections and molar attenuation coefficient of small gold nanoparticles and experimental observation of their UV-vis spectral properties. *Spectrochimica Acta. Part A, Molecular and Biomolecular Spectroscopy*, *191*, 513–520. <https://doi.org/10.1016/j.saa.2017.10.047>
- Tanioka, N., Maeda, H., Shimizu, S., Munekage, M., Uemura, S., & Hanazaki, K. (2021). Indocyanine green fluorescence-guided laparoscopic deroofing of a liver cyst: A case report. *Asian Journal of Endoscopic Surgery*, *15*, 359–362. <https://doi.org/10.1111/ases.12999>
- Tolcher, A. W., & Mayer, L. D. (2018). Improving combination cancer therapy: The CombiPlex. *Future Oncology*, *14*(13), 1317–1332. <https://doi.org/10.2217/fon-2017-0607>
- Tong, S., Zhu, H., & Bao, G. (2019). Magnetic iron oxide nanoparticles for disease detection and therapy. *Materials Today (Kidlington)*, *31*, 86–99. <https://doi.org/10.1016/j.mattod.2019.06.003>
- Upputuri, P. K., Das, D., Maheshwari, M., Yaowen, Y., & Pramanik, M. (2020). Real-time monitoring of temperature using a pulsed laser-diode-based photoacoustic system. *Optics Letters*, *45*(3), 718–721. <https://doi.org/10.1364/OL.386173>
- Vera, J., & Bayazitoglu, Y. (2008). Gold nanoshell density variation with laser power for induced hyperthermia. *International Journal of Heat and Mass Transfer*, *52*, 564–573. <https://doi.org/10.1016/j.ijheatmasstransfer.2008.06.036>
- Wadajkar, A. S., Dancy, J. G., Roberts, N. B., Connolly, N. P., Strickland, D. K., Winkles, J. A., Woodworth, G. F., & Kim, A. J. (2017). Decreased non-specific adhesivity, receptor targeted (DART) nanoparticles exhibit improved dispersion, cellular uptake, and tumor retention in invasive gliomas. *Journal of Controlled Release*, *267*, 144–153. <https://doi.org/10.1016/j.jconrel.2017.09.006>
- Wang, X., Gao, X., & Liu, J. (2010). Monte-Carlo simulation on gold nanoshells enhanced laser interstitial thermal therapy on target tumor. *Journal of Computational and Theoretical Nanoscience*, *7*(6), 1025–1031. <https://doi.org/10.1166/jctn.2010.1448>
- Weissleder, R. (2001). A clearer vision for in vivo imaging. *Nature Biotechnology*, *19*(4), 316–317. <https://doi.org/10.1038/86684>
- West, C. L., Doughty, A. C. V., Liu, K., & Chen, W. R. (2019). Monitoring tissue temperature during photothermal therapy for cancer. *Journal of Bio-X Research*, *2*(4), 159–168. <https://doi.org/10.1097/JBR.0000000000000050>
- Wierzbinski, K. R., Szymanski, T., Rozwadowska, N., Rybka, J. D., Zimna, A., Zalewski, T., Nowicka-Bauer, K., Malcher, A., Nowaczyk, M., Krupinski, M., Fiedorowicz, M., Bogorodzki, P., Grieb, P., Giersig, M., & Kurpisz, M. K. (2018). Potential use of superparamagnetic iron oxide nanoparticles for in vitro and in vivo bioimaging of human myoblasts. *Scientific Reports*, *8*(1), 3682. <https://doi.org/10.1038/s41598-018-22018-0>
- Wolfbeis, O. S. (2015). An overview of nanoparticles commonly used in fluorescent bioimaging. *Chemical Society Reviews*, *44*(14), 4743–4768. <https://doi.org/10.1039/c4cs00392f>
- Wu, X., Ming, T., Wang, X., Wang, P., Wang, J., & Chen, J. (2010). High-photoluminescence-yield gold nanocubes: For cell imaging and photothermal therapy. *American Chemical Society Nano*, *4*(1), 113–120. <https://doi.org/10.1021/nn901064m>
- Xu, X., Meade, A., & Bayazitoglu, Y. (2011). Numerical investigation of nanoparticle-assisted laser-induced interstitial thermotherapy toward tumor and cancer treatments. *Lasers in Medical Science*, *26*(2), 213–222. <https://doi.org/10.1007/s10103-010-0828-3>
- Yaroslavsky, A. N., Schulze, P. C., Yaroslavsky, I. V., Schober, R., Ulrich, F., & Schwarzmaier, H. J. (2002). Optical properties of selected native and coagulated human brain tissues in vitro in the visible and near infrared spectral range. *Physics in Medicine and Biology*, *47*(12), 2059–2073. <https://doi.org/10.1088/0031-9155/47/12/305>
- Yin, Y., Ren, Y., Li, H., & Qi, H. (2020). Characteristic analysis of light and heat transfer in photothermal therapy using multiple-light-source heating strategy. *International Journal of Thermal Sciences*, *158*, 106533. <https://doi.org/10.1016/j.ijthermalsci.2020.106533>
- Zhang, H. (2016). Onivyde for the therapy of multiple solid tumors. *Oncotargets and Therapy*, *9*, 3001–3007. <https://doi.org/10.2147/OTT.S105587>
- Zhang, J., Jin, C., He, Z. Z., & Liu, J. (2014). Numerical simulations on conformable laser-induced interstitial thermotherapy through combined use of multi-beam heating and biodegradable nanoparticles. *Lasers in Medical Science*, *29*(4), 1505–1516. <https://doi.org/10.1007/s10103-014-1558-8>
- Zhao, X., Yang, C. X., Chen, L. G., & Yan, X. P. (2017). Dual-stimuli responsive and reversibly activatable theranostic nanoprobe for precision tumor-targeting and fluorescence-guided photothermal therapy. *Nature Communications*, *8*, 14998. <https://doi.org/10.1038/ncomms14998>
- Zharov, V. P., Galitovskaya, E. N., Johnson, C., & Kelly, T. (2005). Synergistic enhancement of selective nanophotothermolysis with gold nanoclusters: Potential for cancer therapy. *Lasers in Surgery and Medicine*, *37*(3), 219–226. <https://doi.org/10.1002/lsm.20223>
- Zou, L., Wang, H., He, B., Zeng, L., Tan, T., Cao, H., He, X., Zhang, Z., Guo, S., & Li, Y. (2016). Current approaches of photothermal therapy in treating cancer metastasis with nanotherapeutics. *Theranostics*, *6*(6), 762–772. <https://doi.org/10.7150/thno.14988>

How to cite this article: Pang, S., Kapur, A., Zhou, K., Anastasiadis, P., Ballirano, N., Kim, A. J., Winkles, J. A., Woodworth, G. F., & Huang, H.-C. (2022). Nanoparticle-assisted, image-guided laser interstitial thermal therapy for cancer treatment. *WIREs Nanomedicine and Nanobiotechnology*, *14*(5), e1826. <https://doi.org/10.1002/wnan.1826>